A simplified correction method for thermocouple disturbance errors in low-conductivity solids under fire exposure

Ian Pope[a*], Juan P. Hidalgo[a], Rory Hadden[b], José L. Torero[c]

[a]The University of Queensland, School of Civil Engineering, Building 49 Advanced Engineering Building, Staff House Road, The University of Queensland, St Lucia QLD 4072 Australia

[b]The University of Edinburgh, School of Engineering, The King's Buildings, Mayfield Road, Edinburgh EH9 3DW, UK

[c]University College London, Department of Civil, Environmental and Geomatic Engineering, 104 Chadwick Building, Gower Street, London WC1E6BT, UK

*Corresponding author: Ian Pope, i.pope@uq.edu.au

Highlights:

- Coupled modelling and experiments highlight factors influencing thermocouple errors.
- Optimising thermocouple orientation and geometry reduces error, but may not eliminate it.
- Simplified correction method developed and validated for inert heat diffusion.
- Correction requires minimal knowledge of boundary conditions and material properties.
- Correction provides good accuracy until complex heat transfer phenomena dominate.

Abstract:

When a thermocouple is embedded in a material of lower thermal conductivity, under certain heating conditions, the presence of the thermocouple can distort the surrounding temperature field. As a result, the measured temperatures may be much lower than the 'undisturbed' temperatures that would exist without the thermocouple. This study presents the results of a sensitivity analysis of key factors influencing this thermal disturbance. A series of heat transfer models and accompanying experiments are used to demonstrate the effects of thermocouple geometry, contact conditions, thermal properties, and heating regime on the temperature measurement error. These tailored finite element models were validated against experiments on vermiculite insulation board, which confirmed the accuracy of the models in simulating the thermal disturbance for inert heating conditions. Also, a simplified version of the finite element model was used to calculate the thermal disturbance error for a number of conditions, and subsequently to predict a range of corrected temperatures for the experimental measurements. This correction method was found to greatly improve the accuracy of the results for inert heating conditions. This method was further tested against experiments on laminated bamboo, which exhibits more complex heat transfer phenomena, and was shown to provide accurate temperature predictions up to the depth of the char layer. Since the method does not account for the effects of moisture in heat transfer, a creep of uncorrected errors could be observed.

Keywords: thermocouple; temperature measurement; thermocouple error; heat transfer; error correction; thermal disturbance; fire; charring

1. Introduction

As the various stakeholders in the construction industry try to balance competing financial, social, and environmental interests, there is a continual drive for innovation. Beyond the basic requirement for structural adequacy of building elements, there is growing pressure for improvements in embodied carbon, thermal and acoustic performance, moisture management, and aesthetic quality. In order to satisfy these conditions, novel construction materials and systems of increasing complexity are being introduced, for which conventional design frameworks may not be applicable. In particular, fire safety frameworks have failed to keep pace with the introduction of new combustible or bio-based building materials, and non-conventional structural systems – leading in some cases to catastrophic consequences.

In order to quantify and predict the fire performance of these building elements, their thermo-mechanical response to fire exposures is defined through appropriately tailored experimentation or standardised test methods. One of the most important components of these experiments is the in-depth temperature profile measurement, which provides insight into the physical and chemical processes occurring within the material, and is critical in validating predictive thermal and thermos-mechanical models. There are numerous examples of this approach in studies across a wide range of materials, such as timber [1, [2], insulation materials [3], and swelling intumescent coatings [4]. In addition to their use in providing information to modellers, internal temperature measurements are routinely used on their own as a quantitative metric or failure criteria in fire safety research and standard testing.

Fire testing standards globally impose critical temperature criteria for specific measuring points within the tested components, on external surfaces, or at the interface between different components [5-[8] – particularly to indicate conditions relevant to the onset of pyrolysis, a risk of ignition, or loss of structural capacity. For example, the Australian National Construction Code requires that the temperature between the surface of a ‘massive timber’ building element and its non-combustible protective covering must not exceed 300 °C for a defined period of heating [8]. Similarly, the Australian standard for classification of the fire performance of external walls [7] requires that temperatures measured at the mid-depth of any combustible layer or cavity in a façade system must not exceed 250 °C for a continuous period of more than 30 seconds. Fire performance testing of timber elements typically includes in-depth temperature measurements that are used to track the progression of the charring front and ‘heated depth’, which are estimated from the movement of isotherms through the timber [9[10]. Temperature measurements for components of a prototype under Standard Fire Test [5] conditions may also be used to calculate the Fire Resistance Level that would be achieved by a corresponding building element [8].

Beyond the application to fire research and testing, in-depth temperature measurements under much lower heat exposures may be used to analyse the thermal performance of building assemblies, including calculation of the “R-value” [11]. Moreover, in-depth temperatures are often used in inverse modelling of well-defined materials to calculate the heat flux on an exposed surface, or to estimate material properties when the heat flux is known. This method is often applied in fire research [3,[12,[13], but is also widely used in manufacturing, industrial processes, and thermal engineering. A commonality of all these applications is the significant diference between the overall thermal conductivity of the thermocouple and that of the substrate

[11]. Furthermore, in all of these cases, accurate measurement of internal temperatures is essential.

Thermocouples of various designs are ubiquitous in research and standard testing due to their durability, versatility, and ability to operate over a wide range of temperatures. While there is a wide range of thermocouple types available, the basic design comprises two narrow wires of different metals that meet at a junction where the actual temperature measurement is taken. These wires are otherwise separated from each other by some kind of electrically insulating material, generally powdered aluminium oxide (Al_2O_3) or magnesium oxide (MgO). The wires and insulation may then be encased in fibreglass or a metal sheath, depending on the durability required, with the junction exposed or also contained within. The ensemble of these features will define the overall thermal properties of the thermocouple.

1.1 Thermocouple disturbance errors and correction methods

There are a number of potential errors inherent to the use of thermocouples for solid-phase temperature measurement, depending on the characteristics of their implementation. In particular, when a thermocouple with a relatively high thermal conductivity (k) is embedded in a material of much lower conductivity, this can induce a disturbance in the temperature field around the thermocouple due to a 'thermal bridging' effect [14]. This causes the material surrounding the thermocouple tip – where the temperature is measured – to be cooled relative to the undisturbed material, as heat diffuses more easily along the thermocouple. As a result, the measured temperatures within the material (T_{TC}) may be much lower than the 'undisturbed' temperatures (T_{un}) that would exist without the presence of the thermocouple. This effect has been recognised in fire research [1[15[16], but much of the work in quantifying or correcting the error has been developed in the context of industrial applications such as metal casting [17], water quenching [18], and nuclear engineering [19]. Beck [14] described this phenomenon for the case of a thermocouple – represented as a solid cylinder – embedded perpendicular to the heated surface in a material of lower thermal conductivity. Through this analytical study, Beck found that this temperature disturbance can be very significant when the thermal properties of the thermocouple are not close enough to those of the surrounding material, even exceeding 50 % of the undisturbed temperature rise. Beck defined the problem in terms of a series of non-dimensional parameters, of which the most critical was the ratio of conductivities, K, followed by the ratio of the products of density (ρ) and specific heat capacity (C_P) of each material, C:

$$K = \frac{k}{k_{TC}} \qquad \text{and} \qquad C = \frac{\rho C_P}{(\rho C_P)_{TC}}$$

Beck developed a method to predict and correct the measurement error for this specific geometry [14[19], but with a number of simplifying assumptions. In addition to the idealisation of the thermocouple as a homogeneous cylinder, Beck assumed perfect thermal contact with the surrounding material, which was taken to be a semi-infinite body. At some point ahead of the thermocouple tip, a plane normal to the thermocouple is heated by a heat flux that is time-variable but constant in space. Behind the heated plane, thermal properties must remain constant with temperature, and only inert heat conduction through the thermocouple and embedding material is considered. This method of correcting measured temperatures, which is described in

detail by Beck [14[19] and more recently by Woolley and Woodbury [17], involves a numerical inverse convolution procedure to find a correction kernel function that can be used to predict the undisturbed temperatures. Firstly, the transient heat transfer problem is solved numerically for a constant arbitrary surface heat flux, in order to produce a set of artificial values for T_{TC} and T_{un}. These simulated temperatures are then used in the inverse convolution to compute the correction kernel values. If material properties remain constant, then the correction kernel function is independent of the variation in surface heat flux over time, so the correction can be calculated without prior knowledge of the true time-variable surface heat flux. Finally, these correction kernel values are used in the forward convolution to predict the real T_{un} from the measured T_{TC}.

While this method is effective, and has been demonstrated successfully for relatively simple materials and geometries [17], its applicability in fire testing is limited by its simplifying assumptions. For example, assuming perfect thermal contact may be unrealistic in practice, where internal thermocouples are typically inserted into holes drilled into a material or assembly. Due to the practical constraints of machining tolerances and material imperfections, there is likely to be a contact resistance or small air gap between the thermocouple and embedding material. This is particularly relevant for soft or porous materials, such as insulating foams, which inherently contain air gaps and for which it may not be feasible to minimise contact resistance by applying a higher contact pressure at the interface with the thermocouple. The assumption of a uniform surface heat flux is also challenged in many fire testing scenarios, particularly when measurements are needed close to the heated surface of more complex materials or assemblies. In these cases, the heat transfer interactions between the tested components, thermocouples, and the external conditions, may be highly non-uniform. Finally, modelling inert heat conduction with constant thermal properties is often inappropriate for the high thermal loads relevant to fire testing. Under high heat fluxes, many materials of interest undergo physical and chemical processes, such as pyrolysis, swelling, shrinking, cracking, and mass transport, which can affect the internal thermodynamics. The relationships between a thermocouple, its embedding material, and the external boundary conditions, are summarised in Fig. 1.

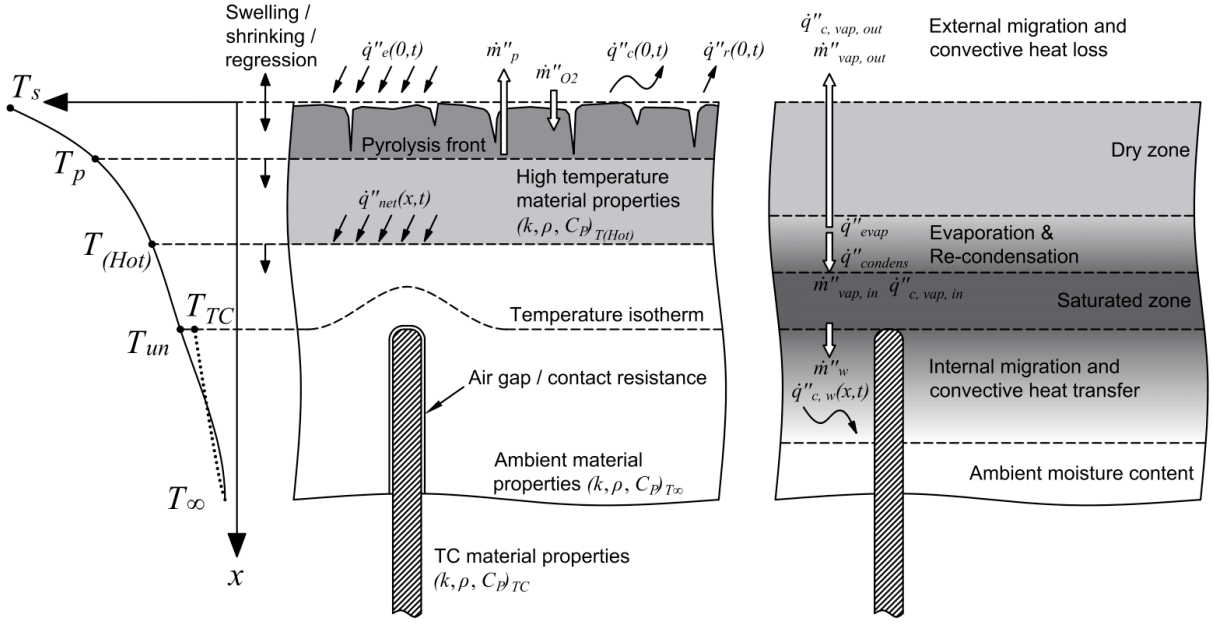

Fig. 1. Summary of key phenomena that can influence temperature measurements and proposed correction methods for a thermocouple inserted perpendicular to the heated surface. Typical boundary conditions, as well as chemical and physical changes are described on the left, with the specific effects of moisture migration, evaporation and re-condensation shown on the right.

As shown in Fig. 1, the externally applied heat flux $\dot{q}''_e(0,t)$, convective heat loss $\dot{q}''_c(0,t)$, and radiative heat loss $\dot{q}''_r(0,t)$ contribute to the exposed surface boundary condition, and all may vary with space and time. The surface itself may shift due to swelling, shrinking, cracking, or ablation of the substrate. Chemical and physical changes in the substrate can substantially change its thermal properties, and may present additional heat sources or sinks. Many materials undergo pyrolysis and oxidation reactions, involving the transport of pyrolysates ($\dot{m}''_p$), and oxygen ($\dot{m}''_{O2}$). The boundary of pyrolysing material is often approximated by an isotherm at a critical temperature (T_p). Even below this temperature, where changes in the chemistry and geometry of the substrate are negligible, there may be changes in the thermal properties (k, ρ, C_P) above ambient temperature. Although these are generally continuously temperature dependent properties (TDP), they are often discretised as constant values between specific temperature ranges. These may include an ambient properties zone, where temperatures are close to ambient (T_∞), and a region of high temperature thermal properties, which may be delineated by the pyrolysis temperature (T_p) or some other temperature above which the properties change significantly above ambient ($T_{(Hot)}$). When the conductivity of the thermocouple (k_{TC}) is higher than that of the surrounding material, there will be a depression in the temperatures around the tip of the thermocouple, such that the actual temperature measured by the thermocouple (T_{TC}) is lower than the undisturbed temperature (T_{un}) existing at the same depth (x_{TC}) far away from the thermocouple. Beck's correction method [14[19] is limited to measurements taken behind a plane subjected to a net heat flux $\dot{q}''_{net}(x,t)$, in front of which all of these complex processes may occur, but behind which only inert heat diffusion and constant thermal properties are accounted for.

Fig. 1 also describes several effects that the presence of moisture can have in a porous medium under a high heating rate, including endothermic evaporation, mass transfer, convective heat transport, and re-condensation. While these phenomena actually occur in a continuous manner through the volume, they are represented simply here as fluxes imposed across discrete boundaries. As the heat wave progresses through the substrate, it evaporates and frees bound water, resulting in an endothermic heat sink (simplified as a heat flux $\dot{q}''_{evap}$). This forces some water out via the surface of the material ($\dot{m}''_{vap,\,out}$) with an associated loss of sensible heat ($\dot{q}''_{vap,\,out}$), while some of the vapour travels deeper into the material ($\dot{m}''_{vap,\,in}$) where it recondenses, transferring both sensible heat and the latent heat of vaporisation ($\dot{q}''_{vap,\,in}$, $\dot{q}''_{condens}$). Eventually, a saturated layer builds up as the pores of the substrate fill. The saturated layer gradually moves deeper, along with a nearby region of higher than ambient moisture content, transporting a mass flux of water ($\dot{m}''_w$) that alters the effective local thermal properties and heats up the surrounding material through convection ($\dot{q}''_{c,\,w}(x,t)$). These phenomena are particularly troublesome for correction methods, because they occur at relatively low temperatures – up to ~100 °C – and absorb large enthalpies, which means that they may have an important effect at significant distances from the heated surface of a material. Furthermore, when moisture migration and accumulation in-depth is possible, these effects may increase in severity with distance behind the heated surface as the saturated layer grows [20]. Crucially, since these phenomena are strongly temperature dependent and transient, they cannot be accounted for in

a model without well-defined material properties and representative boundary conditions. A further complication is the potential for the thermocouple hole to alter the local moisture transport, creating a path for moisture to travel along the thermocouple – whether it is inserted perpendicular or parallel to the heated surface.

Given the limitations in correcting the thermocouple temperature disturbance for a material with complex behaviour, Beck [14] recommended inserting thermocouples parallel to the heated surface, in order to minimise the thermal bridging effect near the tip. While this configuration has been shown to reduce the thermal disturbance significantly [16[17], there is still an appreciable effect, which is dominated by the heat capacity ratio, C [21]. Nevertheless, fire testing standards state that internal temperatures should be measured by taking the thermocouple wires along an isotherm for a distance of at least 50 mm from the junction "where possible", with no additional correction advised [5]. This requirement is often unfeasible for tested systems unless the thermocouple is installed during assembly – a restriction for independent investigation. There are significant practical constraints when positioning thermocouples parallel to the heated surface of a pre-fabricated sample, particularly for large-scale experimentation. If the thermocouple can only be inserted via a drilled hole, it may be impossible to drill a sufficient distance in from the sample side, such that the measurement point is at the desired position. For example, for a wall specimen with a heated surface having a length scale in the order of metres, and a thickness in the order of centimetres, it is unrealistic to position a thermocouple at a point close to the centre of the specimen when drilling from the side, while this can be achieved easily by drilling from the back. Moreover, drilling parallel to the heated surface even on a small scale can result in significant error in the actual distance of the end of the hole from the heated surface. As demonstrated by Reszka [1], a misalignment in the drilling angle of only 5 ° over a length of 50 mm can result in an error in the distance from the heated surface of 4.4 mm when drilling from the side, compared with 0.2 mm from the back. This would result in a potential error margin of ± 4.4 mm in distance from the heated surface when drilling from the side, while this error can only be positive when drilling from the back – resulting in much less uncertainty.

For laminated timber, Farhni *et al.* [15] recommend only inlaying thermocouples between lamellae, parallel to the heated surface. Aside from the need to install the sensors during fabrication, this severely constrains the locations at which thermocouples can be positioned, particularly when the thickness of lamellae is large. Terrei *et al.* [22] also studied this problem for wood, and proposed a solution for small samples, in which the sample is cut in half and thin wire thermocouples are inlaid in machined grooves between the two re-joined halves of the sample. However, an additional complication for thermocouples installed parallel to the heated surface – whether inserted into a drilled hole or inlaid – is that the location of these sensors may change over time if the material surrounding them shrinks or swells under heating. A thermocouple perpendicular to the heated surface may not be disturbed as easily by a swelling or shrinking front traversing the embedding material.

1.2 Proposed simplified correction method

Considering the practical constraints and additional sources of error associated with installing thermocouples parallel to a heated surface, it is worthwhile developing a simplified method of correcting thermocouple disturbance errors that can be applied more broadly in fire research.

This thermocouple disturbance error will be referred to as *E(x,t)*, which can be defined as a percentage by the relative difference in temperature rise above ambient measured by a thermocouple in comparison to the undisturbed temperature rise, as given by Eq. (1).

$$E(x,t) = \frac{(T_{un}(x,t) - T_{TC}(x,t))}{(T_{un}(x,t) - T_{\infty})} \tag{1}$$

If the error history of a thermocouple is known, the experimentally measured thermocouple readings can then be 'corrected' simply by rearranging Eq. (1) and solving for $T_{un}(x,t)$. This is simple enough for a well-defined experimental setup, where a heat transfer model can be constructed to calculate the error using material properties and heating conditions that are known *a priori*. However, in most practical scenarios, either the heating conditions or the variation with time of the temperature-dependent thermal properties of the components may be unknown or poorly defined. These uncertainties may be effectively addressed through sensitivity analyses that bound the relevant parameters.

As observed in previous work by the authors [16], the exact magnitude of the net heat flux at the surface does not have a direct effect on the percentage error (*E(x,t)*) when material thermal properties are constant. Rather, the relative change in the net heat flux in space and time affects the evolution of the resulting error curve. This is analogous to the Beck correction method, in which the correction kernel function is insensitive to the real value of the surface heat flux [14[19]. Generally, the net heat flux on a surface exposed to fire conditions will not remain constant or uniform, but will vary as a function of heat losses from radiation and convection as the surface temperature rises, and with the evolution of the applied heat flux. In many cases, the evolution of the net surface heat flux is unknown – particularly when the surface temperature is likewise unknown – and its determination through inverse modelling may be the original purpose of the temperature measurement [17]. This problem can be simplified through a sensitivity analysis of the terms that control the relative variation in the surface heat flux over time – specifically, the externally imposed heat flux and the surface heat losses ($\dot{q}_l''$). Since the precise magnitude of the net heat flux is irrelevant, the external heat flux ($\dot{q}_e''$) can be given an arbitrary constant value of 1 kW/m^2 in the sensitivity case models. The surface heat losses will be linearised for simplicity, and the heat transfer coefficients for radiation (h_r) and convection (h_c) combined into a total heat loss coefficient (h_l):

$$\dot{q}_l'' = h_c(T_s - T_\infty) + \varepsilon\sigma\left(T_s{}^4 - T_\infty{}^4\right) = h_c(T_s - T_\infty) + h_r(T_s - T_\infty) = h_l(T_s - T_\infty) \tag{2}$$

This total heat loss coefficient can be varied between a 'low heat loss' (LHL) value and a 'high heat loss' (HHL) value.

The value of $\dot{q}_l''$ may vary across the surface, particularly when a thermocouple close to the surface induces a localised temperature depression. Taken to their extremes, these heat loss terms approach conditions of uniform surface heat flux ($\dot{q}_l'' \to 0$) and uniform surface temperature ($\dot{q}_l'' \to \infty$), which respectively induce the maximum and minimum temperature disturbances [14]. Combined with a constant external heat flux, these sensitivity cases are

applicable to scenarios in which a material is undergoing continuous heating, approaching a steady state.

In addition to the variation in the net surface heat flux, the thermal disturbance is governed by the material properties of the different components (reflected by K and C), and their geometries. While the geometries of the thermocouple and the hole are expected to be known within a small error margin, the evolution of temperature-dependent thermal properties over time may not be, especially when the heat flux is unknown. This may also be addressed through a sensitivity analysis, by modelling a range of constant thermal properties for each of the components, associated with different temperature ranges. This is the approach used by Woolley and Woodbury [17] in their application of Beck's correction method.

The proposed correction method involves the application of this sensitivity analysis to an inert heat transfer model that incorporates the specific geometry of the thermocouple and embedding materials. Using the artificial boundary conditions and material properties of the sensitivity analysis, a series of error histories can be calculated, which can directly be used with the experimentally measured temperatures (T_{TC}) to predict a range of corrected temperatures (T_{corr}). As with Beck's method, phenomena that change the geometry of the substrate, or which provide additional heat sources or sinks, cannot be accounted for once they reach the depth of the thermocouple. However, this method is mathematically simpler than the previous correction methods, and allows for consideration of variable surface heat fluxes. Calculation of $E(x,t)$ from the heat transfer model also allows a more realistic representation of the interactions between the thermocouple, its hole, and the embedding material, since these can each be represented as separate components.

This study presents an experimental and modelling examination of the factors influencing the thermal disturbance error and the proposed correction method. The initial investigation is carried out for the heating of vermiculite insulation board, a relatively simple and well-defined material that is commonly used in fire experimentation and industrial processes. Following this validation process, the correction method is then applied to laminated bamboo, a combustible, charring material with increasing relevance as a sustainable future building material. Both of these materials are porous, with a small equilibrium moisture content under ambient conditions. The effects of the moisture are not accounted for in the models, but their impact will be observed in the experiments for comparison.

2. Experimental materials and methods

A series of experiments were conducted in order to explore the sensitivity of the thermocouple disturbance error to a range of practical variables. In these experiments, samples of vermiculite insulation board or laminated bamboo were subjected to constant radiant heat fluxes of either 5 or 60 kW/m^2 from a Mass Loss Calorimeter [23] for 20 minutes. These heat fluxes were chosen to replicate thermal boundary conditions that are representative of potential fire exposures. Moreover, each heat flux will induce distinct ranges of temperature-dependent thermal properties in the component materials, with the higher heat flux resulting in a much steeper temperature gradient across the sample. The samples, with dimensions of 90 × 90 × 50 mm, were oriented vertically, with the radiant heat flux applied horizontally on one face as shown

in Fig. 2. The vertical orientation was chosen to allow thermocouples to be easily inserted via either the back or side of the sample, without being obstructed by the sample holder on the bottom surface. For the laminated bamboo samples, the heat flux was applied perpendicular to the grain. All sides of the sample except the exposed face were covered with ceramic paper insulation and reflective aluminium tape, to block irradiation of the sides of the sample and to minimise heat losses. This insulation was also used to shield the thermocouples from radiation where they extended out from the sample side.

Holes were drilled in either the back or side of the sample to allow the insertion of thermocouples either perpendicular or parallel to the heated surface. For simplicity, thermocouples that are inserted parallel to the heated surface are often referred to as 'side-inserted' thermocouples throughout this paper, while thermocouples oriented perpendicular to the heated surface are called 'back' or 'rear-inserted' thermocouples. These holes were drilled such that the tips of the thermocouples would be either 3 or 20 mm from the exposed surface. The holes were drilled with either a uniform diameter, with a small air gap surrounding the thermocouple along its entire inserted length, or with a stepped diameter, such that the final 9 mm of the hole had the same diameter as the thermocouple. The 9 mm distance was chosen arbitrarily, but it allowed a tight fit to be achieved around the tip of the thermocouple, without the friction becoming too great to fully-insert the thermocouple. For the side-inserted thermocouple case (parallel to the heated surface), holes were drilled 45 mm into the side of the sample in a staggered arrangement, as shown in Fig. 2. For rear-insertion (perpendicular to the heated surface), holes were drilled in a circle of 20 mm radius, such that there was at least 20 mm separation between the centrelines of each thermocouple. In either configuration, the tips of all of the thermocouples were within 20 mm of the centreline of the sample, at least 25 mm from the sides. The thermocouples used in each experiment were either 1.0 mm or 1.5 mm in diameter, with holes drilled to a diameter of either 1.5 mm or 2.0 mm depending on the tightness of fit to be achieved around the thermocouple tip.

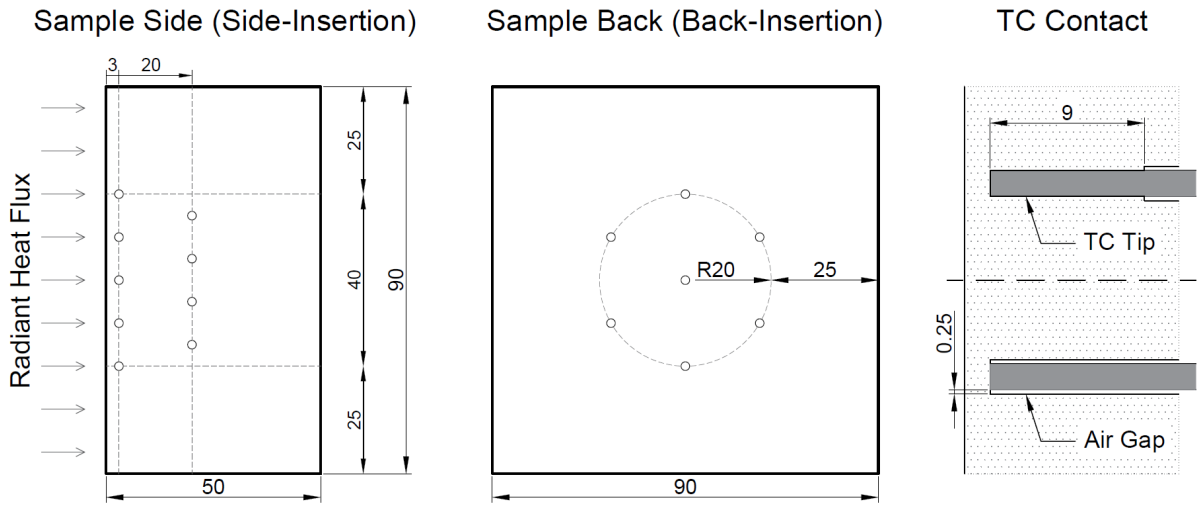

Fig. 2. Placement of thermocouples in tested samples in each orientation, with different tip contact conditions (dimensions in mm).

Mineral-insulated metal-sheathed type K thermocouples with insulated junctions were used to measure the temperatures at each depth within the vermiculite samples. These were composed

of chromel and alumel thermocouple wires, surrounded by magnesium oxide powder insulation within an Inconel 600 sheath. One thermocouple was dissected, so that the dimensions of the sheath and wires could be measured. From these measurements, the relative sizes of the cross-sectional areas of each component of the thermocouple were calculated in proportion to the total thermocouple area. These fractional areas of 55 % for the sheath, 41 % for the MgO, and 4 % for the wires, were then used to calculate weighted-average values for the conductivity and density of the thermocouple from the individual material properties shown in Fig. 3. Since the exact MgO density was unknown, the properties of MgO with a solid volume fraction of 65 % have been used in this calculation as a sensitivity case, since the conductivity of 98 % dense MgO is relatively similar to that of Inconel 600. A weighted-average value for heat capacity was calculated based on the relative mass fractions of each component. The properties of the vermiculite board and laminated bamboo are also shown in Fig. 3.

Samples of the vermiculite board and laminated bamboo were weighed and then dried in an oven at 103 °C for a period of three days, after which time they were weighed again. This indicated a moisture content of 1.1 % by mass for the vermiculite, and 7.4 % for the laminated bamboo.

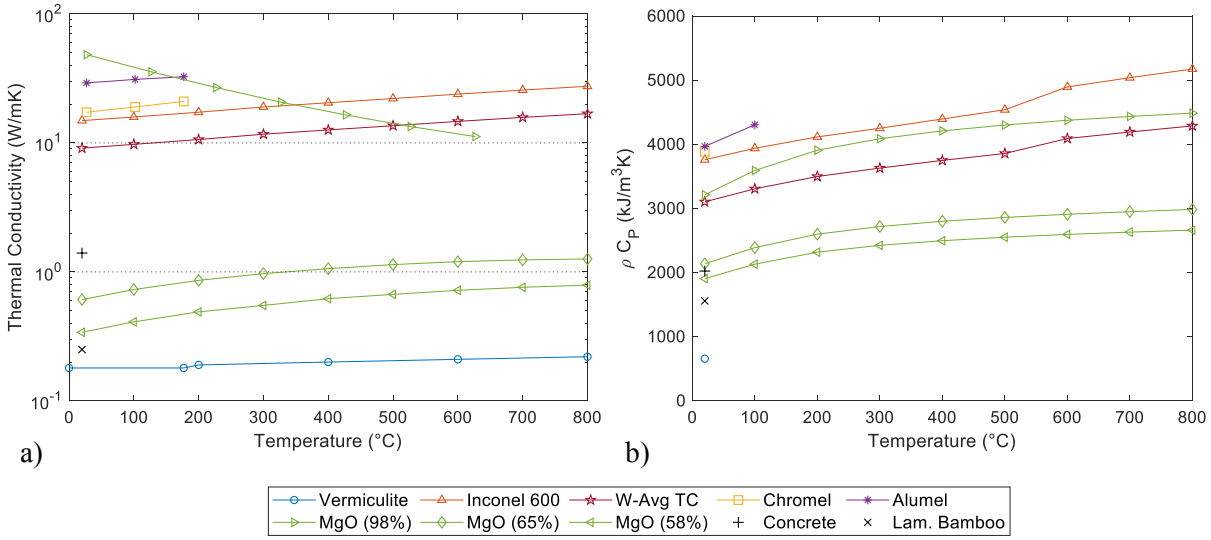

Fig. 3. Thermal conductivities and ρC_P values of thermocouple components and embedding materials over relevant temperature ranges.

As noted in Section 1.1, there is often an error in the placement of the end of a hole drilled parallel to the heated surface due to slight misalignment of the drilling angle. To limit the impact of this error, all vermiculite samples that had thermocouples inserted from the side were cut in half at the end of the experiment, so that the actual position of the end of the hole relative to the heated surface could be measured. This could not be done for the bamboo samples, since the charring of the heated material distorted the geometry. The maximum error in the location of the centreline of a hole was found to be approximately 1.3 mm, corresponding to an error in the drilling angle of approximately 1.6 ° for a 45 mm hole. The results of any thermocouples found to have been in holes with a placement error of more than 0.75 mm were discarded, and the distances of the remaining holes from the heated surface were averaged for each experiment. This average distance is presented along with the average temperature measurements

throughout Section 4. Despite the omission of results from some misplaced thermocouples, at least three valid measurements were recorded for all of the experimental cases.

The experimental matrix in Table 1 details the specific combination of variable conditions in each case. For all of the cases, measurements were taken at depths of 3 and 20 mm from the heated surface, and all other experimental materials and conditions remained the same. The results from these experiments were subsequently used to evaluate models exploring the sensitivity of the thermal disturbance error to different variables.

Table 1. Experimental matrix

TC Orientation	Heat Flux (kW/m^2)	Embedding Material	TC Diameter (mm)	TC Tip Contact	Experiment Name
Back	5	Vermiculite	1.5	Perfect for 9 mm	Back-5-V-1.5-Exp
	60	Vermiculite	1.5	Perfect for 9 mm	Back-60-V-1.5-Exp
	60	Vermiculite	1.5	Air gap around tip	Back-60-V-1.5-Gap-Exp
	60	Vermiculite	1.0	Air gap around tip	Back-60-V-1.0-Gap-Exp
	5	Lam. Bamboo	1.5	Perfect for 9 mm	Back-5-LB-1.5-Exp
	60	Lam. Bamboo	1.5	Perfect for 9 mm	Back-60-LB-1.5-Exp
Side	5	Vermiculite	1.5	Perfect for 9 mm	Side-5-V-1.5-Exp
	60	Vermiculite	1.5	Perfect for 9 mm	Side-60-V-1.5-Exp
	5	Lam. Bamboo	1.5	Perfect for 9 mm	Side-5-LB-1.5-Exp
	60	Lam. Bamboo	1.5	Perfect for 9 mm	Side-60-LB-1.5-Exp

3. Modelling approach

Each of the vermiculite experiments was replicated with finite element heat transfer models using commercial software. These models were specifically tailored to the experimental conditions in each case, so that they could be directly compared with the experimental measurements. The purpose of this exercise was to validate the accuracy of the models in simulating the thermal disturbance created by a thermocouple, so that the models could be further applied to investigate the sensitivity of this disturbance to a greater range of variables. The tailored modelling was not conducted to replicate the experiments with laminated bamboo, because accurate heat transfer models have not been established for this material at high temperatures when heating is not inert.

Models were run both with and without a thermocouple (and hole) present, so that the ‘disturbed’ thermocouple temperatures and ‘undisturbed’ vermiculite temperatures could be calculated. The models were based on an inert heating regime, with no internal mass transfer, heat generation, or internal radiation, but allowing for temperature dependent thermal properties. This is described by a simplified form of the *heat diffusion equation*, Eq. (3), for the general three-dimensional heating case.

$$\frac{\partial}{\partial x}\left(k\frac{\partial T}{\partial x}\right)+\frac{\partial}{\partial y}\left(k\frac{\partial T}{\partial y}\right)+\frac{\partial}{\partial z}\left(k\frac{\partial T}{\partial z}\right)=\rho C_P\frac{\partial T}{\partial t} \tag{3}$$

For the cases in which a thermocouple was inserted perpendicular to the heated surface, a two-dimensional axisymmetric model was created in Abaqus with the axis of rotational symmetry along the centreline of the thermocouple, as shown in Fig. 4. For the side-insertion case, a three-dimensional model incorporating the entire sample block and thermocouple was created, as shown in Fig. 5. The three-dimensional model was constructed in ANSYS, since more powerful computational resources were available for use with this software. Abaqus and ANSYS are widely used FEM software, and are well validated for inert heat transfer. For the specified conditions, there is essentially no difference in the physical model applied by either software, only in the numerical model, so the choice of one over the other in each case was not expected to influence the results significantly. This was verified by comparing the undisturbed vermiculite temperature results from the different models against each other.

A uniform external heat flux, $\dot{q}_e''$, replicating the irradiation from the cone heater, was applied on the heated surface of the vermiculite, along with convective and radiative cooling. The terms of the net heat flux on the heated surface are detailed in Eq. (4). Since vermiculite is opaque, in-depth radiation was neglected and radiation was treated purely as a surface phenomenon [13[29]. Thus, the net heat flux was imposed as a boundary condition on the exposed elements.

$$\dot{q}''_{net,\,s} = a\dot{q}_e'' - \dot{q}''_{l,r} - \dot{q}''_{l,c} = a\dot{q}_e'' - \varepsilon\sigma\left(T_s{}^4 - T_\infty{}^4\right) - h_c(T_s - T_\infty) \tag{4}$$

The convective heat transfer coefficient, h_c, is dependent on the Nusselt number, *Nu*, as well as the conductivity of the gas, k_g, and the characteristic length of the sample, *L*, as shown in Eq. (5).

$$h_c = \frac{\overline{Nu} \cdot k_g}{L} \tag{5}$$

Due to the vertical orientation of the heated surface, the space-mean value of the convection coefficient was calculated from the empirical correlation for the Nusselt number, as shown in Eq. (6), developed by Churchill and Chu [30] for laminar free convection over a vertical plate. This correlation is applicable for this experimental regime since $Ra < 10^9$ and the surface of the sample is approximately isothermal, due to the near uniformity of the imposed heat flux and the insulation of the side boundaries. The characteristic length was taken as 0.09 m, the vertical length of the heated surface.

$$\overline{Nu} = 0.68 + \frac{0.670Ra^{1/4}}{[1 + (0.492/Pr)^{9/16}]^{4/9}} \tag{6}$$

While the Rayleigh number, *Ra,* is given by:

$$Ra = \frac{g\beta(T_s - T_\infty)L^3}{v\alpha} \quad (7)$$

And the Prandtl number:

$$Pr = \frac{v}{\alpha} \quad (8)$$

Where the acceleration due to gravity, g, and the characteristic length, L, are constant, while the inverse of the film temperature, $\beta = T_f^{-1}$, the kinematic viscosity of the air, v, and the thermal diffusivity of air, α, vary with the film temperature, $T_f = (T_s + T_g)/2$ [13[29[31].

The side and rear boundaries of the vermiculite were modelled as adiabatic, as they were covered in ceramic paper insulation in the experiments. These same boundary conditions were also imposed in the 3D model, except that the externally applied heat flux was attenuated away from the centre, based on a heat flux mapping of the cone heater. As a result, the imposed surface heat flux beyond the central 30 mm radius was reduced by 7.5 % for the nominal 5 kW/m^2 exposure, and by 5 % for a central heat flux of 60 kW/m^2. A thermocouple length of 150 mm was included in both 2D and 3D models, with the far end of the thermocouple maintained at a constant ambient temperature Dirichlet boundary condition. In reality, the thermocouple wires (if not the sheath) will continue much further than this, but it is impractical to extend the modelled control volume beyond this point. The high conductivity of the thermocouple materials results in a Biot number, $Bi << 1$, meaning that the thermocouple temperature will rapidly tend to an ambient value from the point at which contact with the embedding material is lost. Therefore, the assumption of an ambient temperature Dirichlet boundary condition at a distance of 103-120 mm beyond the boundary of the embedding material is reasonable, and provides an upper bound to the prediction of energy conducted away from the tip by the wires. In the rear-insertion model, convective and radiative heat losses from the surfaces of the thermocouple where it extends beyond the rear face of the sample were neglected. This simplification was made to the 2D axisymmetric model because the very small Biot number means that heat losses from radiation and convection will be negligible in comparison to the heat conducted along the thermocouple. For the 3D side-insertion model, the temperature of the thermocouple where it extends beyond the sample is much higher than for the rear-insertion case, so radiative and convective cooling was included along the exposed surface. The value of the Nusselt number for convective cooling of the exposed portion of the thermocouple was calculated from the correlation presented by Churchill and Chu [32] for free convection on a horizontal cylinder:

$$\overline{Nu} = \left\{0.60 + \frac{0.387Ra^{1/6}}{[1 + (0.559/Pr)^{9/16}]^{8/27}}\right\}^2 \quad (9)$$

For the 2D axisymmetric model, a structured quadrilateral mesh of quadratic elements was applied, with elements ranging in size from 0.25 to 2 mm along the radial axis and from 0.25 to 1 mm from the front to the back faces. Due to the geometry of the side insertion case, a free

mesh of quadratic tetrahedral and hexahedral elements was used to create the 3D model, based on the adaptive meshing solution provided by the ANSYS software. The adequacy of the mesh in either case was verified through a sensitivity study that found convergence in the model output close to the value provided by the base model. When the number of elements was approximately doubled, the temperature predicted at the tip of a thermocouple 3 mm from the heated surface differed by less than 0.1 °C for the 2D model, and less than 0.2 °C for the 3D model.

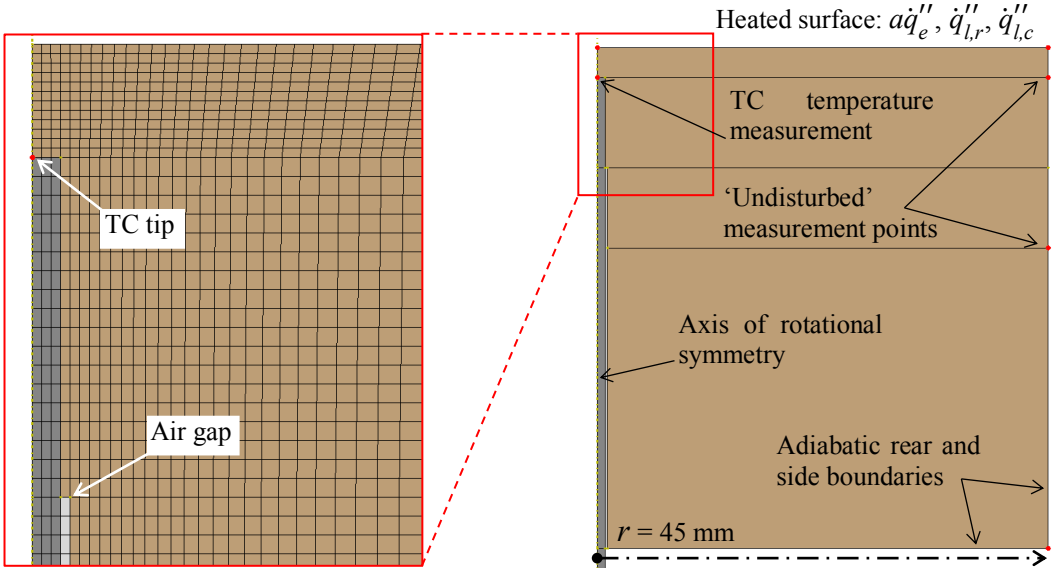

Fig. 4. 2D axisymmetric Abaqus model of TC inserted from the rear of the sample.

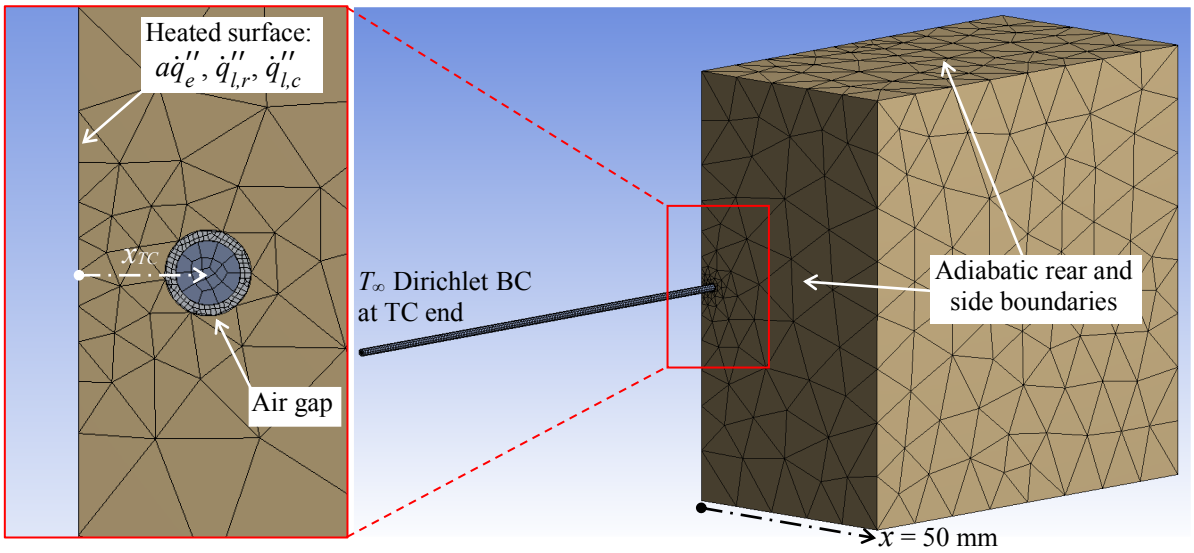

Fig. 5. 3D ANSYS model of thermocouple inserted from the side of the sample.

In each of the models, there is a degree of uncertainty around the thermal properties designated to the various thermocouple components, and their interactions with each other and the embedding material. While the properties of the Inconel sheath and the chromel and alumel

wires are well characterised, the conductivity of the magnesium oxide insulation depends greatly on the packing density of this powder, as seen in Fig. 3, which is difficult to establish post-fabrication. Furthermore, the thermal contact resistances between each of the wires, insulation, sheath and embedding material are unknown, and these values are typically only obtained through inverse modelling. As a simplification, the thermocouple has been implemented in most of the model cases as a solid cylinder with uniform material properties. In the simplest case, the properties of Inconel 600 have been applied to the entire cylinder, since the sheath comprises the majority of the cross-section, and these thermal properties are similar to those of the chromel and alumel wires. Sensitivity cases were also modelled, in which the weighted-average properties of the sheath, wires, and insulation (with a 65 % solid volume fraction) were applied to the entire thermocouple cross-section, as recommended by Beck [14]. This was also compared with a model in which the sheath and insulation were individually represented in the geometry, with their respective thermal properties. In all cases, contact resistance has been neglected, and perfect contact has been assumed between the thermocouple and the embedding material. Where there is an air gap between the sides of the thermocouple and the hole, only conduction through the air has been accounted for, with convection and radiation neglected.

The temperature dependent properties of conductivity, density, and specific heat capacity assigned to the vermiculite, Inconel 600, magnesium oxide, and the weighted-average thermocouple material are given in Fig. 3. The thermal properties of air from Incropera and DeWitt [29] were used for the air gap surrounding the thermocouple, and to calculate the convection conditions on the heated vermiculite surface and the external part of the thermocouple. The radiative properties of the exposed vermiculite surface were determined based on an earlier study of the same material from Laschütza [13], who established the dependencies of total emissivity and spectral absorptivity with temperature and wavelength respectively. Following the approach of Boulet *et al.* [33], the total absorptivity of the vermiculite corresponding to the radiant spectral emission from the cone heater – approximated by a black body – was found to be 0.89 for an incident heat flux of 5 kW/m^2 and 0.75 for 60 kW/m^2. While Laschütza provides temperature dependent total emissivity data, the model software only allowed for a single constant value. Since radiation is most significant at higher temperatures, these inputs were estimated for each incident heat flux based on the highest experimental temperature measurements from thermocouples inserted parallel to the heated surface at a depth of 3 mm. Consequently, emissivity values of 0.91 and 0.80 were selected for external heat fluxes of 5 and 60 kW/m^2, respectively. A summary of the boundary conditions applied for each of the 2D and 3D models – tailored to the specific experimental conditions – is provided in Table 2, while Table 3 outlines the different combinations of variables applied to each of the model cases.

Table 2. Tailored model properties and boundary conditions for vermiculite

Input parameter	2D model (rear insertion)		3D model (side insertion)	
$\dot{q}_e''$ Incident radiation	Uniform over heated surface		Mapped heat flux distribution	
	5 kW/m^2	60 kW/m^2	4.6 - 5 kW/m^2	57 - 60 kW/m^2
T_∞ Ambient temperature	26 °C	26 °C	28 °C	25 °C
Vermiculite (sample surface):				
a_V Absorptivity	0.89	0.75	0.89	0.75
ε_V Emissivity	0.91	0.80	0.91	0.80
$h_{c,V}$ Convective heat transfer coefficient	Empirical relationship for a hot vertical plate in quiescent air [30]			
Sample rear BC	Adiabatic		Adiabatic	
Sample side BC	Adiabatic		Adiabatic	
Inconel 600 (thermocouple length external to sample block):				
ε_{Inc} Emissivity	N/A	N/A	0.7	0.7
$h_{c,Inc}$ Convective heat transfer coefficient	N/A	N/A	Empirical relationship for a hot horizontal cylinder in quiescent air [32]	
TC external end BC	Dirichlet boundary condition at T_∞			
Mesh	Quadratic, quadrilateral Elements: 6089 - 6116 Nodes: 19007 - 19044		Quadratic, tetra/hexahedral Elements: 51916 - 61249 Nodes: 227648 - 240870	

Table 3. Tailored models simulating real boundary conditions and temperature dependent properties of vermiculite

TC Orientation	Heat Flux (kW/m^2)	Diameter (mm)	TC Tip Contact	TC Properties	Model Name
Back (2D model)	5	1.5	Perfect for 9 mm	Inconel only	[B1] Back-5-1.5-Inc-TDP
				Weighted-average	[B2] Back-5-1.5-WAvg-TDP
				Inconel and MgO	[B3] Back-5-1.5-MgO-TDP
	60	1.5	Perfect for 9 mm	Inconel only	[B4] Back-60-1.5-Inc-TDP
				Weighted-average	[B5] Back-60-1.5-WAvg-TDP
				Inconel and MgO	[B6] Back-60-1.5-MgO-TDP
	60	1.5	Air gap around tip	Inconel only	[B7] Back-60-1.5-Gap-TDP
		1.0			[B8] Back-60-1.0-Gap-TDP
		0.5			[B9] Back-60-0.5-Gap-TDP
		2.0			[B10] Back-60-2.0-Gap-TDP
	5	0.5	Air gap around tip	Inconel only	[B11] Back-5-0.5-Gap-TDP
Side (3D model)	5	1.5	Perfect for 9 mm	Inconel only	[S1] Side-5-1.5-Inc-TDP
				Weighted-average	[S2] Side-5-1.5-WAvg-TDP
				Inconel and MgO	[S3] Side-5-1.5-MgO-TDP
	60	1.5	Perfect for 9 mm	Inconel only	[S4] Side-60-1.5-Inc-TDP
				Weighted-average	[S5] Side-60-1.5-WAvg-TDP
				Inconel and MgO	[S6] Side-60-1.5-MgO-TDP

4. Results and discussion

4.1 Evaluation of thermal disturbance

Results from both the models and experiments presented in this section clearly show the disturbance induced by a thermocouple when embedded in a material of much lower conductivity. This is particularly significant when the thermocouple is inserted from the "back", i.e. perpendicular to the heated surface, as seen in Fig. 6. However, this effect can still be seen to a lesser degree when a thermocouple is inserted parallel to the heated surface, as in Fig. 7, since the rear of the thermocouple and the side boundaries of the embedding material are likely to be at a lower temperature than the centre of the sample. This illustrates the importance of ensuring good contact between the thermocouple and the embedding material over an adequate heating length, so that the energy lost through conduction towards the far extent of the thermocouple is minimal in comparison to the energy gained nearer the tip.

4.1.1 Model comparison and validation

In all cases, the models predicted that the temperature at the tip of a rear-inserted thermocouple would be significantly lower than the undisturbed temperature that would exist if no thermocouple was present. This temperature difference is greatest during the transient heating period, but persists even as a quasi-steady state is reached. In both the models and experimental results, the temperatures at the tip of the side-inserted thermocouples were higher than for the rear-insertion case, and were much closer to the predicted undisturbed temperatures. The undisturbed temperature predictions from the two-dimensional axisymmetric Abaqus model matched very closely with those from near the centreline of the three-dimensional ANSYS model. As stated in Table 2, the ambient temperatures for these models differed by up to 2 °C between orientations. Nevertheless, for the different model constructions subjected to 60 kW/m^2 irradiation, the undisturbed temperature results at depths of 3 mm and 20 mm differed by a maximum of 2.5 °C and 3.3 °C respectively, with route-mean-square (RMS) differences of 0.5 °C and 2.5 °C. Under 5 kW/m^2 exposure, the 2D and 3D models differed by less than 2.1 °C and 2.0 °C for each of these depths respectively, with RMS differences of 1.5 °C and 1.7 °C. Considering the relative insignificance of these differences – which are largely explained by the different ambient temperatures in each case – this benchmarking confirmed that the 2D model is effectively equivalent to the 3D model close to the centreline. Away from the centre of the 3D model, temperatures are reduced due to the external heat flux mapping across the surface.

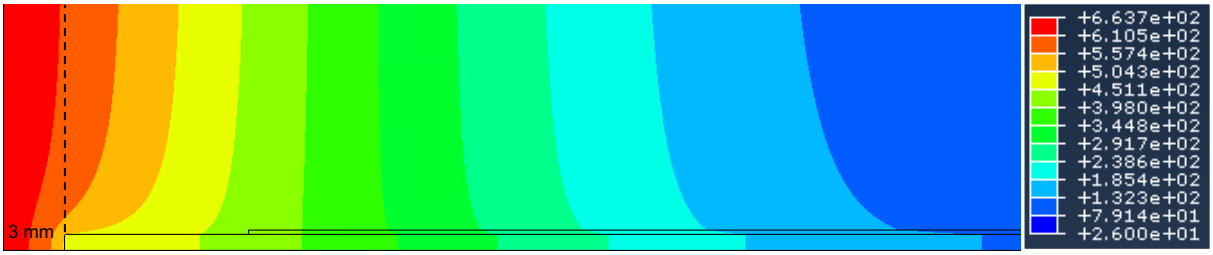

Fig. 6. Graphic from Abaqus model B4 showing the temperature field disturbance induced by a thermocouple inserted perpendicular to the heated surface, at a depth of 3 mm, after 20 minutes of exposure at 60 kW/m^2.

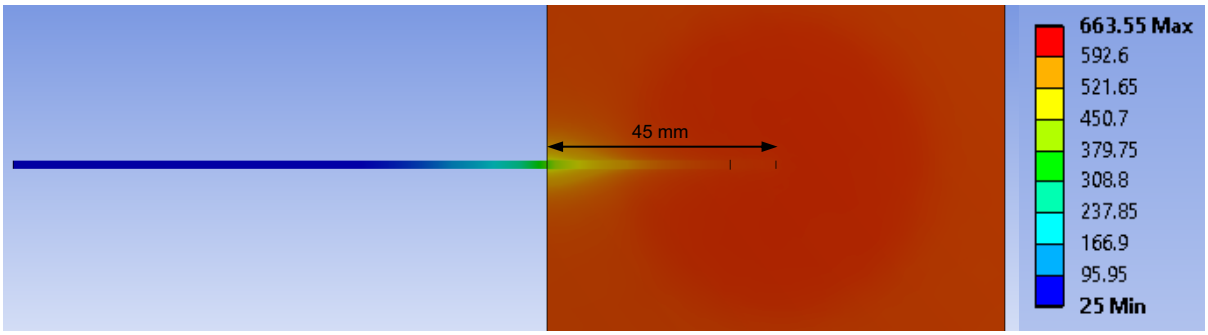

Fig. 7. Graphic from ANSYS model S4 showing a section through a thermocouple inserted parallel to the heated surface, at a depth of 3 mm, after 20 minutes of exposure at 60 kW/m^2.

Fig. 8 displays the results for cases in which a 1.5 mm diameter thermocouple is inserted into a hole with perfect contact between the thermocouple and surrounding vermiculite for 9 mm nearest to the tip. Temperature histories are modelled for the undisturbed case, in which no thermocouple is present, as well as cases where a thermocouple is represented by a solid cylinder of Inconel 600, or as a cylinder with the weighted-average thermal properties of Inconel 600 and magnesium oxide (65 % solid fraction). The cases in which the Inconel thermocouple sheath and MgO core are each included separately (B3, B6, S3, S6) have not been shown in these graphs, since this was found to produce very similar results to the case with weighted-average thermal properties – with a maximum difference of 4.5 °C for 60 kW/m^2 irradiation. This supports the proposition that weighted-average thermal properties can be used to simplify the more complex geometries and interactions between the individual thermocouple components [14]. Similarly, the results of the weighted-average thermocouple properties cases have not been included for the side-insertion cases in Fig. 8 c) and d) for visual clarity, since these results were so close to those of the solid Inconel cases. Experimental measurements (Exp) are presented as averages for each depth, with standard deviation intervals shaded. For the side-inserted thermocouple experiments, the actual average distance between the centrelines of the thermocouple tips and the heated surface is stated on Fig. 8 c) and d).

From observation of the experimental results for thermocouples at a depth of 20 mm, it is apparent that the heat transfer within the vermiculite samples is not truly inert. This is most obvious in the 60 kW/m^2 heating cases, where the temperature measured by the 20 mm thermocouple initially exceed model predictions, before reaching a plateau at around 100 °C. This effect is almost certainly due to the presence of moisture within the porous vermiculite, which was not accounted for in the model. While the relatively small 1.1 % moisture content is not sufficient to produce a significant effect close to the heated surface, as the heat wave travels through the material and forces some of the moisture to migrate inwards [20] it accumulates at greater depths. The migration of this moisture creates an additional convective heat transfer effect, as the hot moisture equilibrates with the relatively cooler surroundings ahead. This would explain the faster than predicted temperature rise up to 100 °C seen for the 20 mm depth in all cases. The other implication of this moisture accumulation is that approaching 100 °C there is a temperature plateau due to the endothermic effect of evaporation. This plateau is likely to become more pronounced with depth, due to the accumulation of moisture and the lower conduction heat flux. This is particularly evident in Fig. 8 b) and d) for 60 kW/m^2 irradiation, but it may also explain why the slope of the experimental temperature histories at 20 mm decrease faster than expected as they approach 100 °C in the 5 kW/m^2 irradiation cases.

Aside from the effect of the moisture, which is outside the scope of this study, the experimental results for rear-inserted thermocouples match very well with the model predictions for a solid Inconel thermocouple. The model predictions for a thermocouple with the weighted-average properties of Inconel and MgO (with a solid fraction of 65 %) are always higher than those for solid Inconel – due to the lower weighted-average conductivity, as shown in Fig. 3. This weighted-average thermocouple model (B2, B5), and the model with a discrete MgO core (B3, B6), appear to overestimate the measured temperatures. This is likely due to the actual solid volume fraction of the MgO being significantly greater than 65 %. The conductivity of MgO powder increases greatly as the solid volume fraction increases from 65 % to 98 %, so any powder with a density towards the upper end of this range will have a conductivity in the same order of magnitude as that of Inconel 600. This explains why the pure Inconel thermocouple model (B1, B4) provides a closer prediction of the experimental results.

As shown in Fig. 8 c) and d), the experimental measurements from thermocouples inserted parallel to the heated surface are slightly lower than those predicted by the models, particularly for the higher heat flux. This is partly due to the fact that the real measured distances of the thermocouple tips were slightly further than 3 mm from the heated surface. As discussed in Section 1, this misplacement is difficult to avoid when drilling thermocouple holes parallel to the heated surface. However, this alone does not fully explain the discrepancy between the modelled and experimental results. Possible explanations are that the thermal properties implemented for either the vermiculite or thermocouple materials do not quite match reality, or that the modelled radiative and convective boundary conditions are not totally representative. Another likely explanation is that the contact conditions between the thermocouple, the vermiculite, and the air gap are not adequately characterised. The assumption of perfect contact between the vermiculite and the tip of the thermocouple was always known to be an overestimate to some degree, due to the unquantified contact resistance between these components. Furthermore, the conduction of heat across the air gap, in which the air has been implemented as an effectively solid component in perfect contact with the adjacent vermiculite and thermocouple, may also be overestimated. The implications of these mischaracterisations are particularly significant for the side-insertion scenario, since the relatively higher temperatures measured by the thermocouple in this case are predicated on efficient heating along the embedded length of the thermocouple. Nevertheless, the results overall suggest that the experimental conditions are represented very well in the models (apart from the moisture effects), particularly for the rear-insertion case.

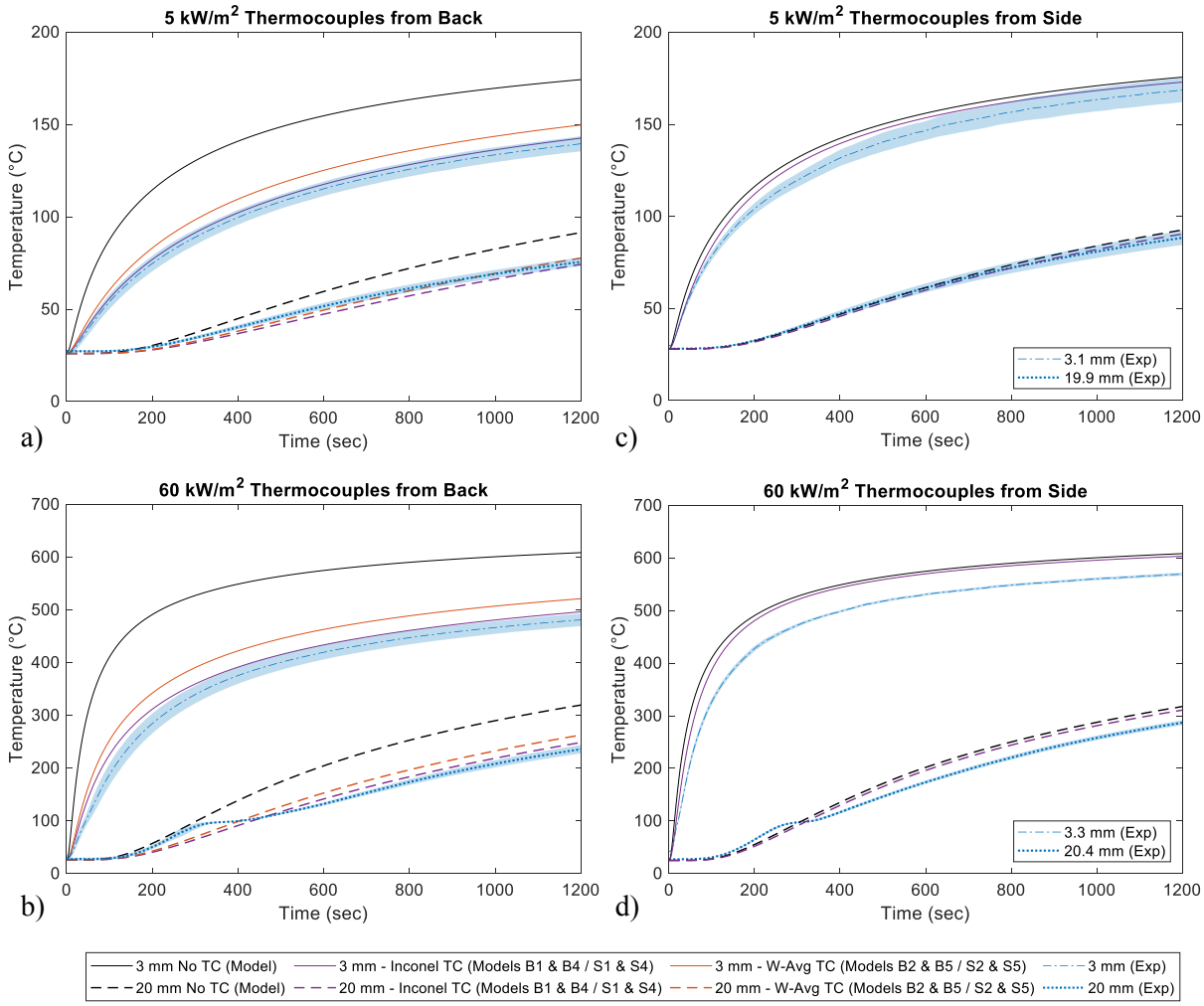

Fig. 8. Modelled and experimental temperature histories for thermocouples inserted from the back or side in vermiculite. Thermocouples are assigned the thermal properties of either solid Inconel or a weighted-average of Inconel and MgO (65 % solid volume fraction). Standard deviation intervals are shaded for experimental results.

In Fig. 9, the results for thermocouples inserted perpendicular and parallel to the heated surface are compared for each heat flux. As in Fig. 8, these results are for the case of a 1.5 mm diameter thermocouple with perfect contact near the tip, but only the models in which thermocouples are represented by a solid Inconel cylinder are included (B1, B4, S1, S4). For simplicity, the undisturbed temperatures displayed in this comparison are those predicted by the 2D axisymmetric model only, since these were found to be very similar to the 3D model results. Fig. 9 clearly illustrates the influence of the thermocouple orientation on the measured temperature results. At both heat flux exposures, the experimental and model results for side-inserted thermocouples are significantly greater than those for rear-inserted thermocouples at each depth. When comparing the mean experimental temperatures in the 60 kW/m^2 exposure case shown in Fig. 9 a), it can be seen that the measurements from side-inserted thermocouples at an average depth of 3.3 mm are up to 143 °C higher than those of the rear-inserted thermocouples at 3 mm after 150 seconds. Even after 1200 seconds, as a quasi-steady state is approached, this gap is 88 °C. The corresponding gap in predictions from modelled thermocouples for these times at a depth of 3 mm are 170 °C and 107 °C, respectively.

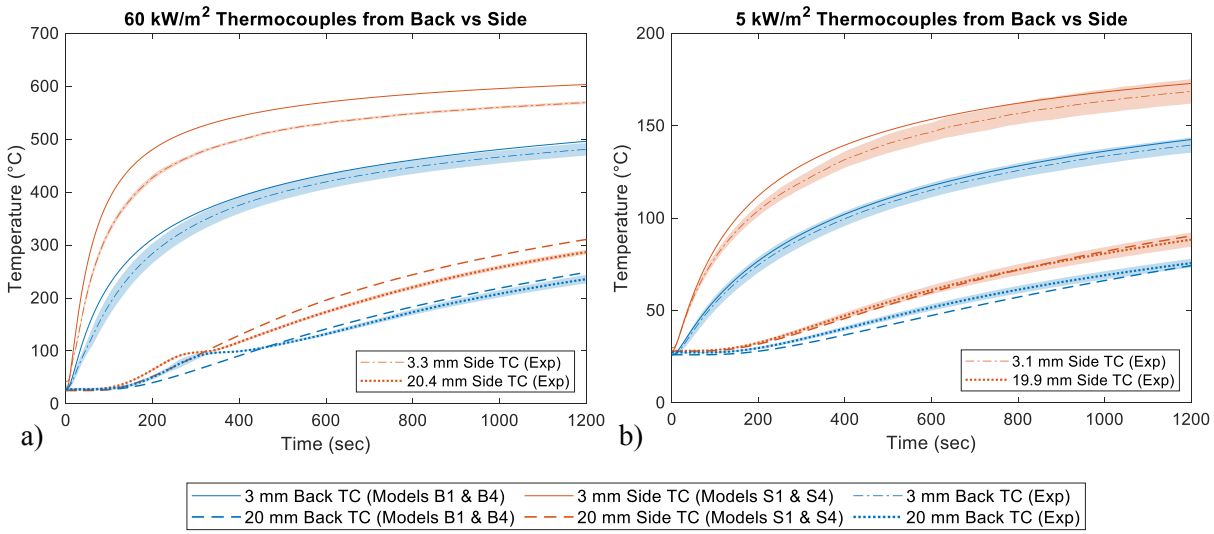

Fig. 9. Comparison between modelled and experimental temperature measurements in vermiculite, with thermocouples inserted from the back or side under 5 or 60 kW/m^2. Standard deviation intervals are shaded for experimental results.

4.1.2 Sensitivity of disturbance to thermocouple geometry

Fig. 10 examines the effects of different a) thermal contact conditions and b) diameters on thermocouples inserted perpendicular to the heated surface. In Fig. 10 a), experimental and model results are presented for a case in which a 1.5 mm diameter thermocouple is inserted into a hole with an equal diameter for 9 mm from the tip of the thermocouple, expanding to a diameter of 2 mm for the rest of the embedded length, as well as a case where the entire length of the hole is 2 mm in diameter. For the model of the "9 mm Contact" case (B4), perfect thermal contact is implemented between the vermiculite and the thermocouple over this length, with conduction across the 0.25 mm air gap for the remainder of the hole. In the second "Air Gap" model (B7), perfect contact between the vermiculite and thermocouple is assumed only at the end of the modelled thermocouple cylinder. Model results reflect the impact of thermal contact efficiency, with higher temperatures predicted when there is perfect contact between the thermocouple and the embedding material than when there is an air gap surrounding the full length of the thermocouple. However, this effect is not clearly seen in the experimental results, for which the average temperatures measured in each case are almost identical (standard deviation intervals have been omitted for visual clarity). Instead, the experimental measurements for both geometries almost exactly match the model predictions for the case with a consistent air gap along the length of the hole. This is likely due in part to the previously mentioned omission of an undetermined contact resistance between the thermocouple and the embedding material. In reality, even a thermocouple inserted into a hole of equal diameter will not conduct heat perfectly with the surrounding material, due to ridges and bumps on each surface creating additional air gaps [29]. This is further exacerbated by the likelihood that the thermocouple and hole geometries do not exactly match in practice, as they are defined by machining tolerances. As such, it is likely that the model of a thermocouple surrounded by an air gap for its full length (B7) is a more realistic representation of both experimental conditions.

In Fig. 10 b), model results for thermocouples of 0.5, 1.0, 1.5 and 2.0 mm diameter are presented, along with experimental results for 1.0 and 1.5 mm diameter thermocouples. In all of the model and experimental cases, the thermocouples are inserted into holes with a diameter

that is 0.5 mm wider, such that there is always a 0.25 mm air gap around each thermocouple for the full embedding length. Experimental results fit very well with the model predictions for this configuration, which together show how thermocouple diameter affects the temperatures recorded. A thermocouple of smaller diameter has less capacity as a thermal bridge to disturb the surrounding temperature fields in the embedding material, since the energy conducted along the thermocouple will be proportional to its cross-sectional area. Therefore, the temperature at the tip of a smaller diameter thermocouple will be closer to T_{un} than would be the case for a larger thermocouple. For the models presented, the 0.5 mm thermocouple is predicted to reduce the thermal disturbance error significantly when compared with a 1.5 mm diameter thermocouple (with a cross-sectional area nine times greater). Nonetheless, even a 0.5 mm diameter thermocouple, which may be the smallest that can practically be used, is predicted to measure temperatures that are still significantly lower than T_{un}. For the 3 mm depth under 60 kW/m^2 irradiance, this difference is predicted to reach a maximum of 123 °C in the first 90 seconds, before approaching a quasi-steady difference of around 57 °C.

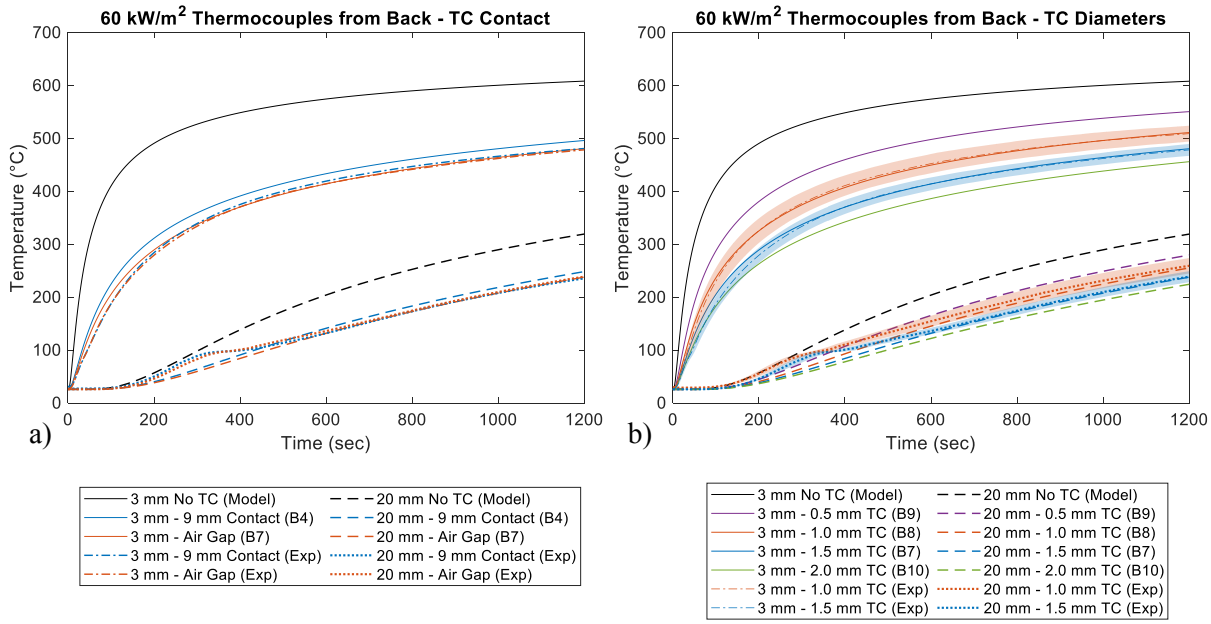

Fig. 10. Effect of thermocouple a) contact conditions, and b) diameter on temperatures measured by a rear-inserted thermocouple in vermiculite.

4.2 Error correction for vermiculite

When analysing the magnitude of the thermal disturbance effect in each case, the predicted and experimentally measured thermocouple temperatures must be compared with an undisturbed reference value, T_{un}. This reference value has been taken to be the temperature of the embedding material at each depth as calculated by the Abaqus model with no thermocouple (or hole) present. It must be acknowledged that there is an uncertainty associated with this, as the undisturbed temperature is controlled by the accuracy of the model, and cannot be experimentally determined. This is the underlying problem that this study is addressing, as it can be seen that even measurements from thermocouples inserted parallel to the heated surface will carry some error – whether due to misplacement or a smaller thermal-bridging effect. For these reasons, the experimental results from side-inserted thermocouples have not been used as reference temperatures for the purpose of quantifying errors, but they are useful as a qualitative

benchmark. Despite this uncertainty, the accuracy of this simple model in predicting the experimentally measured results suggests that these undisturbed temperature predictions are close to reality – aside from the effects of the moisture at lower temperatures. Using this reference, the measurement error of a thermocouple can then be calculated as a proportion of the rise in temperature above ambient predicted for the undisturbed case, as shown in Eq. (1).

The correction method described in Section 1.2 has been applied to the experimental results of the rear-inserted thermocouples shown in Fig. 9. In this process, sensitivity cases are selected to bound the range of possible values for thermal properties and external boundary conditions. The total heat loss coefficient from Eq. (2) is varied between a 'low heat loss' (LHL) value of 10 W/(m^{2}K) and a 'high heat loss' (HHL) value of 80 W/(m^{2}K), which respectively correspond to near-ambient and high (~800 °C) surface temperatures in this experimental configuration. These heat loss conditions were combined with an arbitrary constant external heat flux of 1 kW/m^2 to constitute the thermal boundary conditions for the sensitivity cases.

In the scenarios examined in this study, two cases bound the spectrum of possible values for the conductivity ratio, *K*, which could be present during different stages of heating. Firstly, the 'ambient properties' case (Amb), in which all material properties are kept constant at their ambient temperature values. This is most representative of the earliest stage of heating, when the thermocouple and the surrounding material are yet to heat up significantly, or when the imposed heat flux is low and temperatures do not rise significantly above ambient. Secondly, an upper bound value for *K* results from the 'high temperature material properties' case (Hot), where the thermal properties of the embedding materials are taken to be their values at a high temperature, but the thermocouple properties remain at their ambient levels. For the vermiculite experiments, the thermal properties at 700 °C were used as an upper bound.

By running the simple 2D axisymmetric model with different combinations of inputs from the extreme cases described above, a range of possible error evolutions was computed from the model temperature outputs for a 1.5 mm diameter thermocouple. These sensitivity cases are outlined in Table 4.

Table 4. Sensitivity case models for vermiculite, with linearised heat losses and constant thermal properties

TC Orientation	Heat Losses	Diameter (mm)	TC Tip Contact	Material Properties	Model Name
Back (2D model)	'Low' 10 W/(m^{2}K)	1.5	Perfect for 9 mm	Ambient Inconel and Vermiculite	C1 Back-LHL-1.5-Amb
				Ambient Inconel, "Hot" Vermiculite	C2 Back-LHL-1.5-Hot
	'High' 80 W/(m^{2}K)	1.5	Perfect for 9 mm	Ambient Inconel and Vermiculite	C3 Back-HHL-1.5-Amb
				Ambient Inconel, "Hot" Vermiculite	C4 Back-HHL-1.5-Hot

The error curves calculated from these sensitivity models are bounded by two extreme cases. The highest errors predicted are for the 'ambient properties' case with low heat losses (C1), while the lowest predicted thermal disturbance error results from the 'hot vermiculite properties' case with high heat losses (C4). The errors calculated for each of these cases are shown in Fig. 11, along with the errors calculated by the high fidelity models (B1, B4) presented in Table 3 that include the true external heat fluxes, heat losses, and temperature-dependent thermal properties. Despite the range in thermal properties and heating conditions, the predicted errors for each thermocouple depth remain relatively close, with the two extreme cases differing by less than 10 % at any given time. As would be expected, the sensitivity case with constant ambient temperature properties and relatively low surface heat losses (C1) closely approximates the error predictions from the 5 kW/m^2 external heat flux model, since the maximum material temperature predicted by this realistic case is only 191 °C at the surface. The error curve predicted by the 60 kW/m^2 external radiation model (B4) is bounded on the lower side by the other extreme of a model with hot vermiculite properties and relatively high surface heat losses (C4). The 'hot vermiculite properties' case becomes less appropriate at greater depths, as the temperature of the vermiculite near the thermocouple tip is much lower than that assumed for this model. Nevertheless, the application of these sensitivity cases – which required only details of the experimental geometry and broad ranges of thermal parameters – has effectively bounded the real error curves. This provides a useful tool in estimating 'corrected' thermocouple temperatures, without prior knowledge of exact boundary conditions. Moreover, the bounds of this sensitivity analysis can be narrowed through further iterations once an initial correction is made.

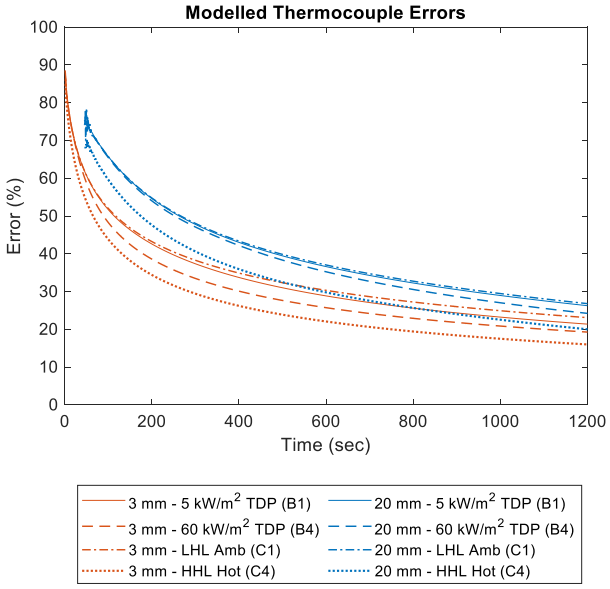

Fig. 11. Relative thermocouple errors, $E(x,t)$, calculated from tailored models with temperature-dependent properties and precisely replicated boundary conditions (B1, B4), compared with the sensitivity case models with constant material properties, an arbitrary incident heat flux, and 'low' or 'high' surface heat losses (C1, C4).

Fig. 12 shows the evolution of the relative error resulting from different distances between the tip of a rear-inserted thermocouple and the heated surface. There is an initial delay as the heat wave first reaches each depth, before the error decreases in an approximately logarithmic fashion with over time. As the heat wave first disturbs the temperatures at each depth, the relative error is initially high, and extremely sensitive to tiny changes in temperature (<< 1 °C).

As such, there may be a need to truncate the beginning of the calculated errors, particularly when small fluctuations in the measured temperatures (due to the sensitivity limits of real thermocouples) can be much larger than temperature rises predicted in the model.

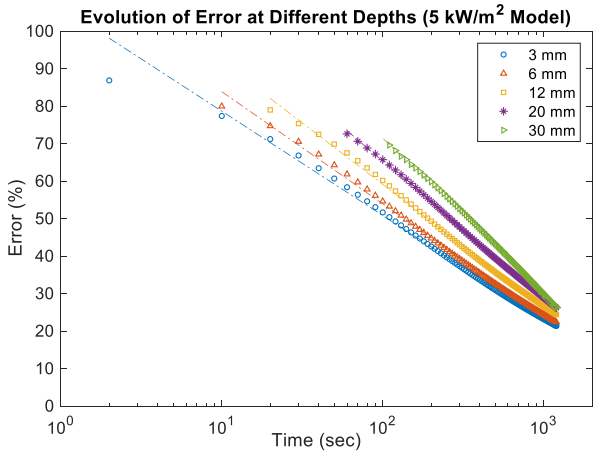

Fig. 12. Relative errors calculated from model B1 for various distances between the thermocouple tip and heated surface. Logarithmic regressions are fitted for each data set (dash-dot lines) with R^2 values greater than 0.99.

4.2.2 Accuracy of corrected results

Using the error histories shown in Fig. 11 and the experimentally measured thermocouple temperatures as inputs, Eq. (1) can be rearranged to estimate the undisturbed temperatures at the corresponding depths. These 'corrected' thermocouple results are shown in Fig. 13 a) and b). The corrected results from the tailored models with temperature-dependent properties (B1, B4) are presented as individual lines, alongside shaded areas that are bounded by the corrections calculated from the two extreme sensitivity case models (C1, C4). In general, the corrected thermocouple results provide a good approximation of the modelled undisturbed temperatures, and the corrected measurements from all of the sensitivity cases show a significant improvement on the uncorrected rear-inserted thermocouple results. The main deficiency in these model corrections is that they do not account for the effect of the moisture at lower temperatures and greater depths, as described in Section 4.1.1. In reality, the effects of moisture migration and evaporation dominate over the thermal-bridging effect up to 100 °C. Since this is not accounted for in the models, the corrected results are less accurate for the duration of these moisture-related phenomena at each depth. This can be seen most clearly in the results of the 20 mm deep thermocouple for the 60 kW/m^2 irradiation experiment, where the corrected results significantly overestimate the real temperatures until the moisture evaporation plateau – which in reality must occur around 100 °C – has passed. The moisture effect is difficult to deal with quantitatively, since any implementation of moisture diffusion and evaporation in the model would depend on the real temperatures within the embedding material. While this could be achieved for a model with well-defined thermal properties and heating conditions, it is not feasible in the 'blind' sensitivity cases.

The corrected results could be further improved if the exact contact conditions between the thermocouple and embedding material were more accurately characterised in the model. All of the models used to calculate the corrected temperatures assumed perfect thermal contact around the tip of the thermocouple, but in reality, there will be some degree of contact resistance that

will reduce the thermocouple tip temperature. This was previously identified as a likely reason why the model tended to slightly over-predict the experimental thermocouple temperatures. Implementing more representative thermal contact conditions in the model would improve the accuracy of the corrected temperature estimates.

To illustrate the benefit of the correction, errors have been calculated for the 'corrected' results from each of the sensitivity cases, by replacing T_{TC} in Eq. (1) with the corrected temperatures T_{Corr}. In Fig. 13 c) and d), these errors are compared with those from the uncorrected experimental thermocouple results for rear-insertion, as well as the predicted error from a modelled side-inserted thermocouple (S1, S4) at a distance of 3 mm behind the heated surface. The errors calculated for the sensitivity cases have been separated into different two shaded bands based on models with ambient material properties (C1, C3), and those with hot vermiculite properties (C2, C4). These bands are delineated at their upper and lower bounds by models with high and low surface heat losses respectively. In Fig. 13 c), the calculated errors for the thermocouple 20 mm behind the heated surface were very significantly impacted by the moisture effects, so these results have been presented only from the end of the moisture evaporation plateau at 400 seconds. The results for the 20 mm thermocouples in the 5 kW/m^2 heating case were less severely affected by the moisture, since temperatures at this depth did not reach the 100 °C moisture plateau. However, the calculated errors for this location, presented in Fig. 13 d), are very unstable before 150 seconds, since the oscillations in the experimental thermocouple readings can be greater than the predicted temperature rise in this period. Prior to this time, the tailored model (B1) predicts a temperature difference between T_{TC} and T_{un} of less than 1 °C, so any errors before this time are of no real significance and have not been presented.

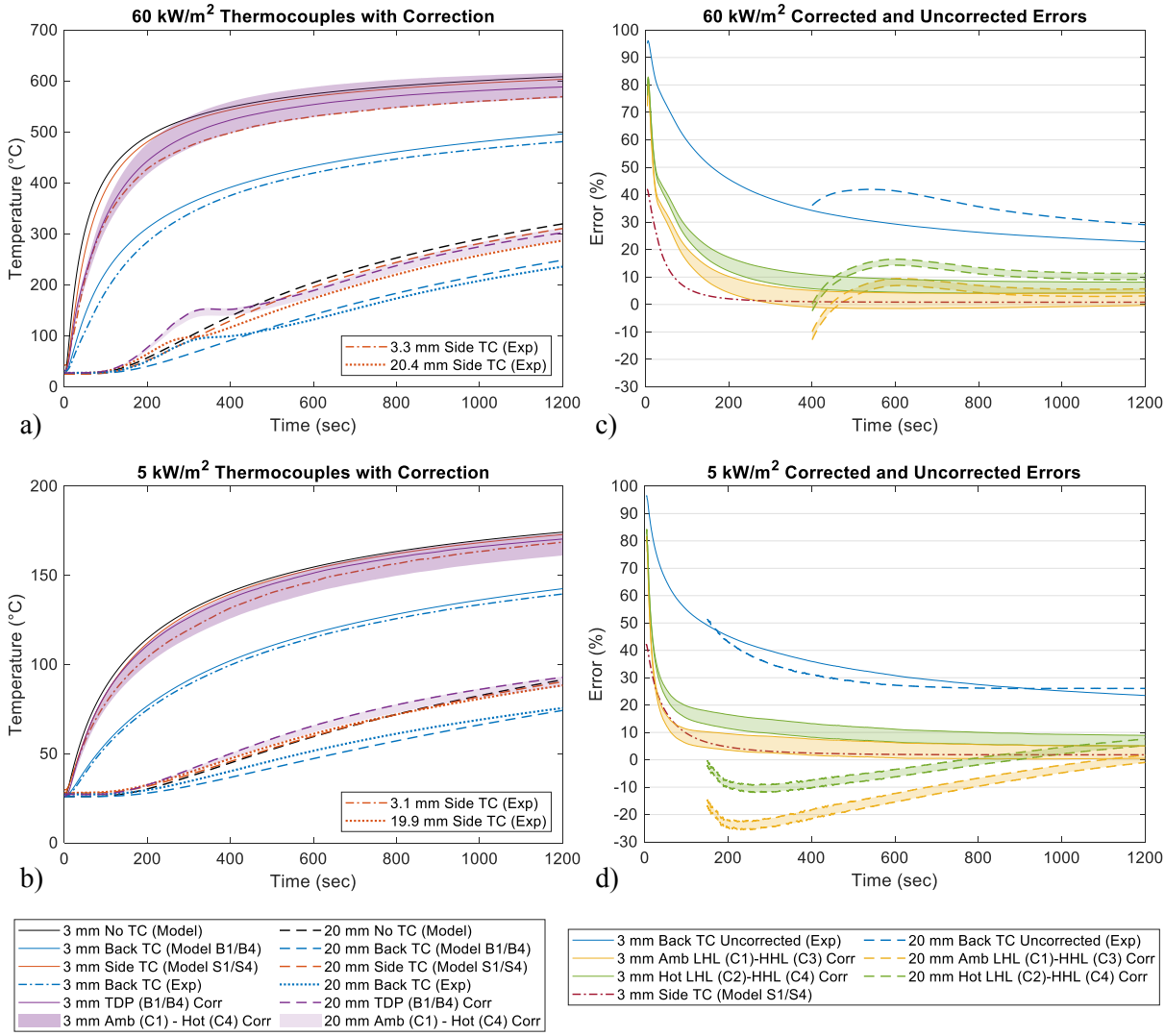

Fig. 13. Comparison between corrected and uncorrected thermocouple measurements for a) 60 kW/m^2 and b) 5 kW/m^2, and the corresponding errors calculated for 'corrected' and uncorrected measurements in c) and d). The shaded areas are bounded by the sensitivity cases C1, C2, C3, and C4.

The corrected results for rear-inserted thermocouples from all of the modelled sensitivity cases show a significant reduction in error over the uncorrected experimental measurements for all times, apart from the periods when the effects of the moisture are most dominant. Relative errors are still quite large in the moment when the heat wave first reaches each depth, but this corresponds with only relatively small absolute differences in temperature at these times, and the error subsequently drops rapidly. As shown in Fig. 13 c) and d), this high early error is also apparent in the model predictions for side-inserted thermocouples. This suggests that the corrected rear-inserted thermocouple results are of comparable value even before potential tip positioning errors in the side-inserted thermocouples are considered.

As a means of comparing the value of the correction method, the route-mean-square (RMS) errors of the 'corrected' results from each case (B1/B4, C1, C2, C3, C4) have been calculated over the periods shown in Fig. 13 c) and d). These errors are shown in Fig. 14, along with the errors calculated for uncorrected experimental measurements, and for the uncorrected temperatures predicted by the tailored models (B1/B4). The corrected results, which all apply

to a thermocouple of 1.5 mm diameter, are also compared with uncorrected model predictions for a 0.5 mm diameter thermocouple in a 1.0 mm hole (B9/B11). From this comparison, it is apparent that the corrections made from the 'blind' sensitivity case models still provide comparable accuracy to the corrections from the tailored models with real surface heat fluxes and temperature-dependent properties. Moreover, these corrections are also an improvement on the expected accuracy of an uncorrected 0.5 mm thermocouple, although this may not always be the case when heat transfer through the material is not solely governed by inert conduction – e.g. when moisture effects dominate.

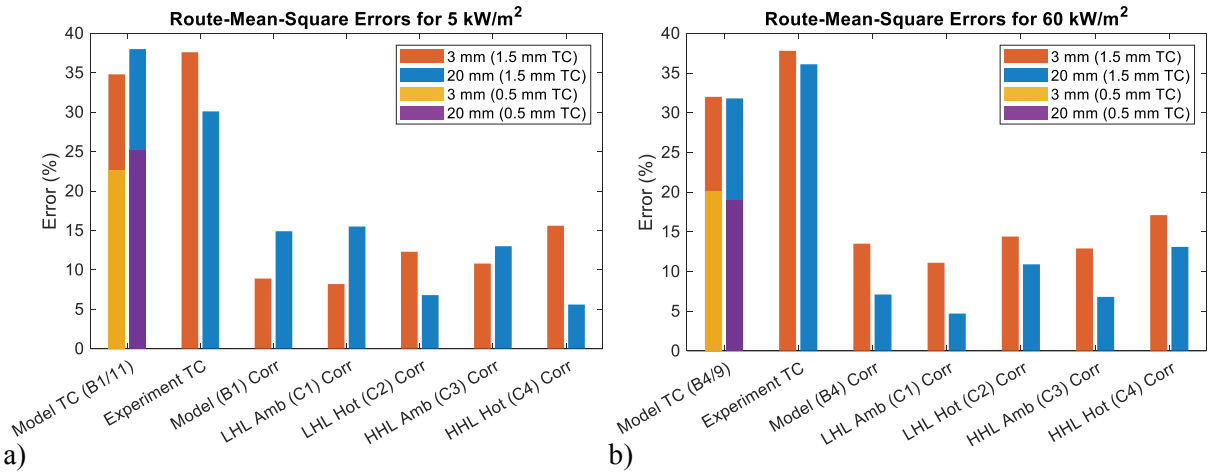

Fig. 14. Comparison of RMS errors for corrected and uncorrected modelled and experimental temperatures measured with a rear-inserted thermocouple of either 0.5 or 1.5 mm diameter. For the 20 mm depth, the RMS error is calculated for the truncated periods as shown in Fig. 13 c) and d).

4.2.3 Summary of correction process and limitations

The analysis in Section 4.2.2 has shown how relatively simple finite element modelling, based on sensitivity cases with only minimal knowledge of thermal properties and heating conditions, can be used to calculate corrected temperature measurements within accurate ranges. Within this study, these results have been benchmarked against experimental measurements from thermocouples inserted perpendicular or parallel to the heated surface, and against models that have been tailored to the precise experimental conditions. Given the relative accuracy of corrections calculated from these 'blind' sensitivity case models, this method could be applied to other experimental scenarios in which thermal properties and exposure conditions are not previously well-established. For a new material 'X', subjected to an unknown heat load, this process would be as follows:

1. Construct a heat transfer model that replicates the geometry and estimated contact conditions of each thermocouple embedded within material X, as well as the boundary conditions of the unexposed surfaces.
2. Estimate values for thermal properties that correspond to the extreme temperature conditions that could be reached.
3. Create model sensitivity cases that assign different combinations of the extreme thermal properties to each of the embedding material and the thermocouple components. These cases should encompass the highest and lowest expected values for the conductivity ratio, K, and the heat capacity ratio, C.

4. Impose a constant arbitrary surface heat flux for the period over which continuous heating is observed from the uncorrected measurements.
5. For each sensitivity case, apply a range of surface heat loss coefficients that correspond to estimated ambient and high surface temperature heat losses.
6. For each model, calculate the error history, $E(x,t)$, from the simulated thermocouple and undisturbed temperatures.
7. Use the calculated error history and the experimentally measured thermocouple temperatures to calculate a 'corrected' thermocouple temperature for each sensitivity case. Combined, this will produce a corrected measurement range that can be further narrowed iteratively by adjusting the bounds of the sensitivity cases as appropriate.

While potentially useful in many experimental scenarios where a significant thermal disturbance error cannot be avoided, this method does have some limitations to its applicability and accuracy under certain conditions. Considering that the proposed models are based on heat diffusion purely through inert conduction within the solid phase, any transient effects related to the presence or migration of moisture within a porous solid will not be accounted for. As demonstrated in this study, these effects can reduce the accuracy of the 'corrected' measurements, particularly during the period before measured temperatures exceed 100 °C. This is especially troublesome under conditions where there is a significant plateau in temperatures due to moisture evaporation. Furthermore, this method is applicable for scenarios involving continuous heating, and may need to be adjusted to apply to any cooling periods. These correction models are also applicable only when the embedding material surrounding the thermocouple is a continuous solid, and become invalid if the geometry or contact conditions of the material around the thermocouple are altered due to behaviours such as charring, shrinkage, intumescence or delamination. However, the presence of these phenomena ahead of the thermocouple tip may be permissible, since the relative error is insensitive to the magnitude of the exposure heat flux. The precision of the range of corrected temperatures also depends on how greatly the thermal properties of the embedding material change with temperature. If these properties vary significantly, such that K or C are very different between individual sensitivity cases, the correction range will become much broader.

4.3 External validation - error correction for laminated bamboo

The correction method has also been applied to the measurements from experiments on laminated bamboo samples. Laminated bamboo is a lignocellulosic material, comparable to timber, which undergoes charring at high temperatures. As a result, the thermal properties of the material change markedly as the bamboo is converted into char, with significant decreases in density and conductivity. The pyrolysis reactions that convert bamboo into char occur over a range of temperatures, but the base of the char layer is commonly approximated by the 300 °C isotherm [34]. Above this temperature, shrinking, cracking and oxidation of the char layer limit the applicability of the correction method, so the properties of the char at around 300 °C were taken as the upper bound. Although the thermal properties of bamboo char are not well-established, the authors have previously estimated these based on equivalent values for timber [35]. Following this, the properties for the ambient temperature case for the laminated bamboo experiments were those shown in Fig. 3, while the high temperature properties were designated as k = 0.09 W/m·K, ρ = 133 kg/m^3, and C_P = 1559 J/kg·K. As with vermiculite, low and high heat loss coefficients of 10 and 80 W/m^{2}K were used in the sensitivity cases.

The measured and corrected results for rear-inserted thermocouples are compared with measurements from side-inserted thermocouples in Fig. 15. The average values of the experimental measurements are presented as lines surrounded by shaded standard deviation intervals. In the case of the side-inserted thermocouples, much of the variation is likely due to error in the placement of the tip, as explained in Section 1.1. The corrected temperature ranges – which are calculated for only the experimental averages – are presented as shaded regions bounded by the extreme values of the sensitivity cases. Once again, these results clearly show the significance of the thermal disturbance error for the rear-inserted thermocouples, as temperatures recorded are well below those of thermocouples inserted parallel to the heated surface. For temperatures up to around 300 °C, the corrected results demonstrate a clear reduction of this error, and match closely with the results of the side-inserted thermocouples. At higher temperatures, the accuracy of the corrected results is reduced with the onset of shrinkage, cracking and oxidation of the char layer, particularly above 700 °C as the thermocouples start to become exposed by the receding surface. Nonetheless, the accuracy of predictions up to 300 °C is valuable in quantifying the charring rate and temperature profile below this isotherm, which are necessary for structural analysis under fire conditions.

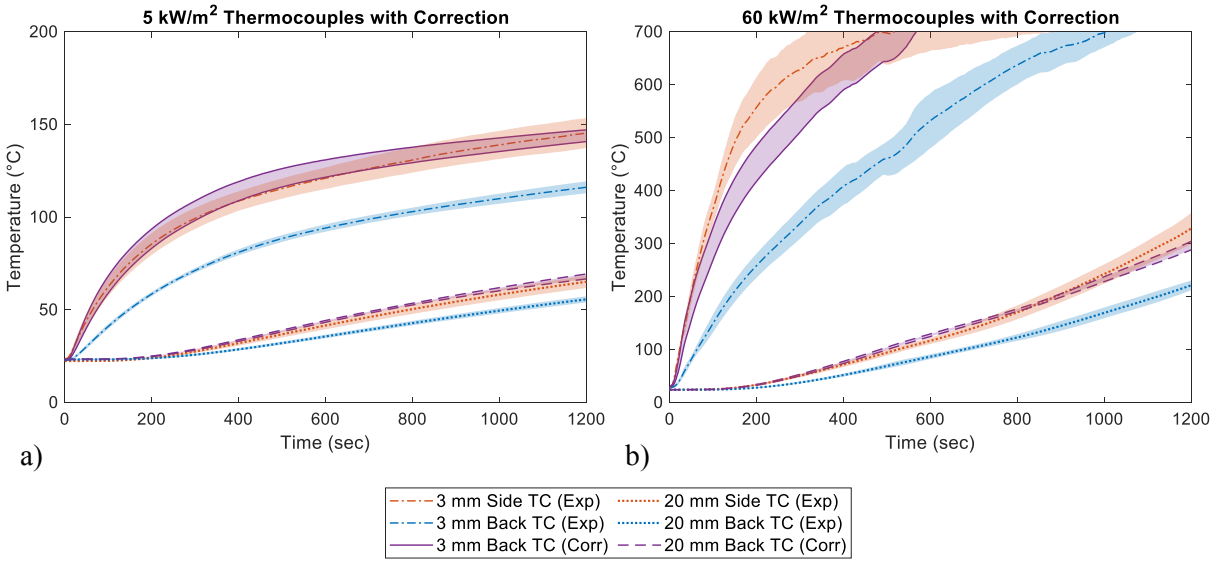

Fig. 15. Corrected and uncorrected thermocouple measurements for laminated bamboo exposed to a) 5 kW/m^2 and b) 60 kW/m^2. Average values for the experimental results are shown with standard deviation intervals shaded. Corrected temperature ranges are bounded by the extreme values of the correction sensitivity cases.

Despite the higher moisture content of laminated bamboo relative to vermiculite, there did not appear to be a significant transient effect of moisture on either the measured or the corrected results. The relatively minor influence of moisture on the heat transfer in laminated bamboo, when heated perpendicular to the grain, has previously been observed by the authors [35]. This is due to the orientation of the fibres and discontinuities in the bamboo lamellae preventing the moisture from continuously migrating and accumulating at greater depths – whereas heating parallel to the grain direction accentuates these effects.

5. Conclusions

This study has presented the results of a sensitivity analysis of key factors influencing the thermal disturbance induced by a thermocouple in a material of lower conductivity. A series of heat transfer models and accompanying experiments demonstrated the effects of thermocouple geometry, contact conditions, thermal properties, and heat flux on the temperature measurement error. These tailored finite element models were confronted with experiments on vermiculite insulation board, which confirmed the accuracy of the models in simulating the thermal disturbance for inert heating conditions. The results clearly illustrate the thermal bridging effect created by a thermocouple inserted perpendicular to the heated surface of a solid. This causes a drop in temperature around the tip of the thermocouple, such that the measured temperature is much lower than the undisturbed temperature that would occur without the presence of a thermocouple. This error can be very large in the early heating period, exceeding 70 % of the undisturbed temperature rise, and may remain significant even as a quasi-steady state is approached.

The disturbance is greatly reduced when the thermocouple is inserted parallel to the heated surface, but the error is not eliminated for the earliest times, and this configuration is often unfeasible in practice. Even when thermocouples can be inserted from the 'side', care must be taken to account for misplacement of the tip or movement due to shrinking or swelling of the substrate. Reducing the diameter of the thermocouple can also minimise the thermal disturbance, but it may still be significant even for a diameter of 0.5 mm.

A simplified version of the finite-element model was used to calculate the thermal disturbance error for a number of sensitivity cases, and subsequently to predict a range of corrected temperatures from the experimental measurements. This process requires minimal knowledge of external boundary conditions or thermal properties of the substrate, which are both varied within representative ranges. This correction method is simpler than Beck's [14], in that it forgoes the inverse convolution procedure to calculate correction kernels. However, like Beck's method, it can only account for inert heat diffusion between the thermocouple and surrounding material. As a result, the correction is only applicable until more complex phenomena such as shrinking, swelling or oxidation reach the depth of the thermocouple. The effects of moisture migration and accumulation under heating may be particularly problematic, because these can have a significant impact on the heat transfer even at relatively low temperatures. Nonetheless, when applied to the measurements of 1.5 mm diameter thermocouples inserted perpendicular to the heated surface, the corrected temperature ranges predicted through this method were a considerable improvement on the experimental measurements. These corrected temperatures had greater accuracy than even a 0.5 mm diameter thermocouple, and were comparable to the measurements from a thermocouple inserted parallel to the heated surface.

Following the success of this simplified correction method for the heating of vermiculite, it was further applied to the more complex heat transfer in laminated bamboo. The additional validation from these experiments reinforced the merits and limitations of the correction method. Despite minimal knowledge of the boundary conditions and material properties, the corrected results matched closely with the side-inserted thermocouples for temperatures up to around 300 °C, below which heating is relatively inert. Above this temperature, the corrected results increasingly diverged as more complex burning behaviours arose. Even with this

limitation, the correction method still allowed for a significant improvement in the accuracy of temperature measurement up to this value, which is highly valuable in quantifying charring rates and degradation of this material under fire exposure.

Acknowledgements

The authors would like to thank the Worshipful Company of Engineers for their financial support, provided through the Sir Peter Gadsden Britain Australia Travel Award 2018. The authors are also grateful to Moso International BV for providing the laminated bamboo.

References

[1] Reszka, P 2008, 'In-depth temperature profiles in pyrolysing wood', PhD thesis, The University of Edinburgh, Edinburgh.

[2] Richter, F & Rein, G 2020, 'A multiscale model of wood pyrolysis in fire to study the roles of chemistry and heat transfer at the mesoscale', *Combustion and Flame*, vol. 216, pp. 316-325.

[3] Hidalgo-Medina, JP 2015, 'Performance-based methodology for the fire safe design of insulation materials in energy efficient buildings', PhD thesis, The University of Edinburgh, Edinburgh.

[4] Lucherini, A 2020, 'Fundamentals of thin intumescent coatings for the design of fire-safe structures', PhD thesis, The University of Queensland, Brisbane.

[5] CEN 2012, *Fire resistance tests – Part 1: General Requirements*, EN 1363-1:2012, European Committee for Standardization, Brussels.

[6] BSI 2020, *Fire performance of external cladding systems*, BS 8414:2020, BSI Standards Limited.

[7] Standards Australia Limited 2016, *Classification of external walls of buildings based on reaction-to-fire performance*, AS 5113:2016, SAI Global Limited, Sydney.

[8] ABCB 2019, *NCC 2019 Building Code of Australia – Volume One*, Australian Building Codes Board, Canberra.

[9] Reszka, P & Torero, JL 2016, 'Fire behaviour of timber and lignocellulose', in Belgacem N & Pizzi A (eds), *Lignocellulosic Fibers and Wood Handbook*, Scrivener Publishing LLC, Beverly, pp. 555-581.

[10] White, RH 2016, 'Analytical Methods for Determining Fire Resistance of Timber Members', in Hurley MJ et al. (eds), *SFPE Handbook of Fire Protection Engineering*, 5th edn Springer, New York, pp. 1979-2011.

[11] Soret, GM, Lázaro, D, Carrascal, J, Alvear, D, Aitchison, M & Torero, JL 2017, 'Thermal characterization of building assemblies by means of transient data assimilation', *Energy and Buildings*, vol. 155, pp. 128-142.

[12] Maluk, C 2014, 'Development and application of a novel test method for studying the fire behaviour of CFRP prestressed concrete structural elements', PhD thesis, The University of Edinburgh, Edinburgh.

[13] Laschütza, T 2017, 'Numerical and experimental investigation of a Thin Skin Calorimeter (TSC)', MSc Dissertation, The University of Edinburgh, Edinburgh.

[14] Beck, JV 1962, 'Thermocouple temperature disturbances in low conductivity materials', *Journal of Heat Transfer*, vol. 84, no. 2, pp. 124-131.

[15] Fahrni, R, Schmid, J, Klippel, M & Frangi, A 2018, 'Correct temperature measurements in fire exposed wood', *2018 World Conference on Timber Engineering*, WCTE 2018 Committee, Seoul, Republic of Korea, 20-23 August.

[16] Pope, I, Hidalgo, JP & Torero, JL 2020, 'A correction method for thermal disturbances induced by thermocouples in a low-conductivity charring material', *Fire Safety Journal*, https://doi.org/10.1016/j.firesaf.2020.103077

[17] Woolley, JW & Woodbury, KA 2011, 'Thermocouple data in the inverse heat conduction problem', *Heat Transfer Engineering*, vol. 32, no. 9, pp. 811-825.

[18] Li, D & Wells, MA 2005, 'Effect of subsurface thermocouple installation on the discrepancy of the measured thermal history and predicted surface heat flux during a quench operation', *Metallurgical and Materials Transactions B*, vol. 36, pp. 343-354.

[19] Beck, JV 1968, 'Determination of undisturbed temperatures from thermocouple measurements using correction kernels', *Nuclear Engineering and Design*, vol. 7, pp. 9-12.

[20] Harmathy, T 1965, 'Effect of Moisture on the Fire Endurance of Building Elements', in A Robertson (ed.), *Moisture in Materials in Relation to Fire Tests*, ASTM International, West Conshohocken, PA, pp. 74-95.

[21] Pfahl, RC, Jr. & Dropkin, D 1966, 'Thermocouple temperature perturbations in low-conductivity materials', *American Society of Mechanical Engineers – Papers*, Paper 66-WA/HT-8

[22] Terrei, L, Acem, Z, Marchetti, V, Lardet, P, Boulet, P & Parent, G 2020, 'In-depth wood temperature measurement using embedded thin wire thermocouples in cone calorimeter tets', *International Journal of Thermal Sciences*, https://doi.org/10.1016/j.ijthermalsci.2020.106686

[23] ISO 1993, *Fire Tests Reaction to Fire Part 1: Rate of Heat Release from Building Products (Cone Calorimeter Method)*, ISO 5660-1:1993, International Organization for Standardization, Geneva.

[24] Special Metals Corporation 2008, *INCONEL alloy 600*, viewed 15 July 2019, <http://www.specialmetals.com/assets/smc/documents/alloys/inconel/inconel-alloy-600.pdf>.

[25] Sundqvist, B 1992, 'Thermal diffusivity and thermal conductivity of Chromel, Alumel, and Constantan in the range 100-450 K', *Journal of Applied Physics*, vol. 72, no. 2, pp. 539-545.

[26] Powell, RW, Ho, CY & Liley, PE 1966, *National Standard Reference Data Series - National Bureau of Standards 8, Thermal Conductivity of Selected Materials*, U.S. Government Printing Office, Washington.

[27] NIST 2018, *Magnesium oxide*, U.S. Department of Commerce, viewed 15 July 2019, <https://webbook.nist.gov/cgi/inchi?ID=C1309484&Type=JANAFS&Plot=on>.

[28] Godbee, HW & Ziegler, WT 1966, 'Thermal conductivities of MgO, Al_2O_3, and ZrO_2 powders to 850°C, I. Experimental', *Journal of Applied Physics*, vol. 37, no. 1, pp. 40-55.

[29] Incropera, FP, DeWitt, DP, Bergman, TL & Lavine, AS 2007, *Fundamentals of heat and mass transfer*, 6th edn, John Wiley & Sons, Hoboken NJ.

[30] Churchill, SW & Chu, HHS 1975, 'Correlating equations for laminar and turbulent free convection from a vertical plate', *Int. J. Heat Mass Transfer*, vol. 18, no. 11, pp. 1323-1329.

[31] Hidalgo, JP, Maluk, C, Cowlard, A, Abecassis-Empis, C, Krajcovic, M & Torero, JL 2017, 'A Thin Skin Calorimeter (TSC) for quantifying irradiation during large-scale fire testing', *International Journal of Thermal Sciences*, vol. 112, pp. 383-394.

[32] Churchill, SW & Chu, HHS 1975, 'Correlating equations for laminar and turbulent free convection from a horizontal cylinder', *Int. J. Heat Mass Transfer*, vol. 18, no. 9, pp. 1049-1053.

[33] Boulet, P, Parent, G, Acem, Z, Collin, A, Försth, M, Bal, N, Rein, G & Torero, J 2014, 'Radiation emission from a heating coil or a halogen lamp on a semitransparent sample', *International Journal of Thermal Sciences*, vol. 77, pp. 223-232.

[34] Bartlett, AI, Hadden, RM, Bisby, LA 2019, 'A review of factors affecting the burning behaviour of wood for application to tall timber construction', *Fire Technology*, vol. 55(1), pp.1-49.

[35] Pope, I, Hidalgo, JP, Osorio, A, Maluk, C & Torero, JL 2019, 'Thermal behaviour of laminated bamboo structures under fire conditions', *Fire and Materials*, https://doi.org/10.1002/fam.2791